VISUAL AND AUDITORY SENSITIVITIES AND DISCRIMINATIONS

AFOSR F49620-97-1-0051

Final Report 15 Dec. 1996 — 14 Dec. 1999

P.I. D. Regan

York University, 4700 Keele St., North York, Ontario, Canada, M3J 1P3

REPORT DOCUMENTATION PAGE

AFRL-SR-BL-TR-00-

0124

PLEASE DO NOT RETURN YOUR FORM TO THE ABOVE ADDRESS.

1. REPORT DATE (DD-MM-YYYY)	2. REPORT DATE	3. DATES COVERED (From - To)
01/03/2000	FEB 2000	12/15/96 to 12/14/99

4. TITLE AND SUBTITLE

VISUAL & AUDITORY SENSITIVITIES & DISCRIMINATIONS

5a. CONTRACT NUMBER

5b. GRANT NUMBER
F49620-97-1-0051

5c. PROGRAM ELEMENT NUMBER

6. AUTHOR(S)

REGAN, DAVID

5d. PROJECT NUMBER

5e. TASK NUMBER

5f. WORK UNIT NUMBER

7. PERFORMING ORGANIZATION NAME(S) AND ADDRESS(ES)

YORK UNIVERSITY
MRS. NOLI SWATMAN RM. S415 ROSS BLDG.,
4700 KEELE ST., NORTH YORK,
ONTARIO, CANADA M3J 1P3

8. PERFORMING ORGANIZATION REPORT NUMBER

9. SPONSORING/MONITORING AGENCY NAME(S) AND ADDRESS(ES)

SPONSORING:
AFOSR/NL
110 DUNCAN AVE., STE. B115
BOLLING AFB, DC, 20332-8080

MONITORING:
AFOSR/NL
801 N. RANDOLPH ST. RM. 732
ARLINGTON, VA 22203-1977

10. SPONSOR/MONITOR'S ACRONYM(S)
AFOSR/NL

11. SPONSORING/MONITORING AGENCY REPORT NUMBER

12. DISTRIBUTION AVAILABILITY STATEMENT

DISTRIBUTION STATEMENT A
Approved for Public Release
Distribution Unlimited

13. SUPPLEMENTARY NOTES

14. ABSTRACT

Errors in judging absolute time to collision using monocular information alone range from 2 to 12% and from 2.5 to 10% using binocular information alone, but only 1.3 to 2.7% using the combination. For small targets, judgements are based entirely on binocular information. (2) Individuals make large errors in judging absolute time to collision with a rotating nonspherical object when judgements are based on monocular information, but not when binocular information is provided. (3) When simulating closure with a textured object, systematic errors in judging time to collision can occur if the rates of expansion of texture element size and object size are not matched exactly. (4) Exposure to expanding images produces errors in judging time to collision that may cause errors in NOE flight and may be a cause of rear-end highway collisions. (5) The human visual system does contain binocular mechanisms sensitive to speed. (6) Simulated objects can be seen and recognized entirely on the basis of texture differences. The physiological limit for locating a texture-defined boundary is 1.7 to 2.4 min are, and visual acuity for texture-defined gratings is above 7 c/deg. Spatial frequency discrimination threshold is approx. 5% for both texture-defined and luminance-defined gratings for frequencies less that 3 - 4 c/deg.

15. SUBJECT TERMS

vision; visual flying skills; camouflage; flight simulators; intersubject differences; visual navigation; perception of motion and self–motion; stereo; brain responses; audition

16. SECURITY CLASSIFICATION OF:			17. LIMITATION OF ABSTRACT	18. NUMBER OF PAGES	19a. NAME OF RESPONSIBLE PERSON
a. REPORT	b. ABSTRACT	c. THIS PAGE			LARKIN, WILLARD
U	U	U	UNLIMITED	106	19b. TELEPONE NUMBER (Include area code) 703-696-7793

1. RESEARCH OBJECTIVES

Listed in the proposal as follows:

1.1 Long Term Aims

1.1.1 We will further develop the channeling hypothesis by: (a) identifying new visual channels; (b) elucidating rules for cue combination in rich visual environments; (c) advancing understanding of eye-limb coordination in skilled visual performance and the role of inter-individual variations of visual sensitivities in limiting skilled visual performance.

1.1.2 We will apply the channeling hypothesis as follows: (a) to inform the design of visual displays in flight simulators so as to improves transfer of training; (b) to provide design criteria for better interfacing night vision aids to the human user's visual system; (c) to inform the design of stereo visual displays used by operators of remotely-controlled vehicles such as unmanned air vehicles or operators of maneuverable land or sea vehicles used to inspect or repair equipment in environments hostile to life; (d) to inform the design of spatially-complex static or dynamic displays such as displays of infra-red, radar or visual imagery; (e) to design tests to screen personnel for their visual competence in specific tasks such as, for example, NOE helicopter flight, low-level aviation over snow-covered terrain, highway driving in high-glare conditions (low sun, approaching headlamps at night).

1.1.3 We will advance our understanding of the auditory processing of complex sounds.

1.1.4 We will use neuromagnetic and evoked potential recording techniques to achieve the following aims: (a) identify the brain sites of different kinds of visual processing and auditory processing, and relate these sites to the organization of visual and auditory areas in macaque monkey cortex; (b) relate objective data on visual and auditory processing in human brain to psychophysical models of human vision and hearing.

1.2 Specific Aims: Visual Psychophysics in Normally-Sighted Individuals

1.2.1 *Perception of texture-defined form and the precision with which texture-defined boundaries are localized*

We will supplement our previous studies of orientation discrimination and letter detection and recognition for texture-defined (TD) form by determining (a) two-dimensional aspect ratio discrimination threshold for a TD rectangle, (b) spatial frequency discrimination threshold for a TD grating and (c) vernier step acuity and bisection acuity for a TD boundary.

1.2.2 *Multiple cues to form*

We will determine the combination rules for texture contrast, motion contrast, luminance contrast and color contrast for (a) the detection of spatial form and (b) the discrimination of orientation, spatial frequency, and two-dimensional aspect ratio.

1.2.3 *Spatial frequency and orientation channels for texture-defined form*

We will find whether the human visual pathway contains multiple parallel spatial filters for TD form.

1.2.4 *Spatial frequency and orientation channels for motion-defined form*

We will find whether the human visual pathway contains multiple parallel spatial filters for motion-defined (MD) form.

1.2.5 *Spatial frequency and orientation channels sensitive to more than one visual dimension*

We will find whether the human visual pathway contains multiple parallel spatial filters that are sensitive to more than one of the following visual dimensions: texture contrast; motion contrast; luminance contrast.

1.2.6 *Monocular judgements of time to collision with an approaching object*

We will measure the absolute accuracy of judging the time to collision with an approaching simulated object for a rigid spherical object and a nonspherical rotating object using monocular cues alone. We will compare findings in the case of a stationary observer and in the case of simulated self-motion. We will also determine how the accuracy of judging time to collision is affected by adaptation caused by pre-exposure to approaching motion and pre-exposure to simulated self-motion. All these experiments will be repeated for objects whose visibility is created by luminance contrast, by texture contrast and by motion contrast.

1.2.7 *Binocular judgements of time to collision with an approaching object*

We will repeat 2.2.6 in the situation that the only available cues to time to collision are binocular cues.

1.2.8 *Judgements of time to collision based on a combination of monocular and binocular cues*

We will repeat 2.2.6 in the situation that both monocular and binocular cues are available in the unique mix characteristic of real-world objects.

1.2.9 *Binocular and Cyclopean processing of the direction of motion in depth*

We will find: (a) whether the direction of motion in depth of a cyclopean target is processed through channels tuned to the direction of motion in depth; (b) whether cyclopean processing can completely account for binocular sensitivity to the direction of motion in depth of a monocularly-visible target; (c) assess intersubject variability in discrimination thresholds for the direction and speed of motion in depth for cyclopean targets.

1.3 Specific Aims: Simulator Studies

1.3.1 Using a helmet-mounted stereo flight simulator we will find the effects on judgements of time to collision and judgements of the direction of self-motion of (a) the degree of mismatch of the dynamics of texture and size of terrain features and (b) density of texture in the visual environment.

1.4 Specific Aims: Brain Recording Studies

1.4.1 *Brain Neurons Sensitive to Cyclopean Form: Tuning Bandwidths for Orientation, Spatial Frequency and Temporal Frequency*

We will measure the orientation tuning bandwidths, spatial frequency tuning bandwidths and temporal frequency tuning bandwidths of cyclopean neurons in human visual cortex by recording responses from the human brain to two superimposed cyclopean grating and using our nonlinear analysis technique.

1.4.2 *Brain Neurons Sensitive to Motion-Defined Form: Tuning Bandwidths for Orientation, Spatial Frequency and Temporal Frequency*

We will repeat 2.4.1 using two superimposed motion-defined gratings.

1.4.3 *Brain Neurons Sensitive to Texture-Defined Form: Tuning Bandwidths for Orientation, Spatial Frequency and Temporal Frequency*

We will repeat 2.4.1 using two superimposed texture-defined gratings.

1.4.4 *Brain Neurons Sensitive to Color-Defined Form: Tuning Bandwidths for Orientation, Spatial Frequency and Temporal Frequency*

We will repeat 2.4.1 using two superimposed equiluminant chromatic gratings.

1.4.5 *Brain Neurons Sensitive to More than One Kind of Contrast*

We will repeat 2.4.1 using a cyclopean grating superimposed on a luminance grating, a texture grating superimposed on a luminance grating, and so on.

1.5 Specific Aims: Auditory Studies

1.5.1 We will extend our theoretical work on the response of auditory hair cells to complex sounds so as to make the work more relevant to speech perception. In particular, we will develop a theoretical treatment of the distortion produced by hair cells on inputs that consist of sums of tones that are modulated in both amplitude and frequency. We will allow for noise and also for adaptive changes in the hair cell transducer characteristic.

1.6 Specific Aims: Development of Operational Screening Tests

1.6.1 *Glare Susceptibility*

We will extend the applicability of our current test for susceptibility to wide-field glare to the case of a point glare source that is close to an object being fixated. Then we will establish inter-individual differences in test results.

1.6.2 *Collision Avoidance*

We will develop a test for determining a pilot's ability to judge the time to collision with an object on a collision course.

2. ACCOMPLISHMENTS / NEW FINDINGS.

2.1 **Visual Processing of Texture-Defined Form**

Relevance: The aim of this line of research is to provide the psychophysical knowledge necessary to evaluate different simulations of ground texture and to better understand the visual processing of ground texture in low-level and NOE aviation.

In all the studies described below we used orientation texture rather than any of the many other kinds of texture. Our choice was based on Nothdurft's evidence [Proc. Roy. Soc. B, 239, 295 - 320, (1990); Vision Res. 31, 299 - 320 (1991)] rejecting blob size, line intersections or "crossings" and line ends or "terminators" as genuine textons. He concluded that, of all the candidate textons he investigated, only orientation differences could, by itself, support texture segregation. He stated that other candidate textons he investigated produced texture segregation artifactually.

2.1. (a) Location judgements for texture-defined boundaries.

Long-Term Aims 1.1.1(b). 1.1.2(a); Specific Aims 1.2.1(c), 1.2.2(a).this project is completed and a paper has been published. Gray R. & Regan, D. (1997). *Vernier step acuity and bisection for texture-defined form.* Vision Research, 37, 1713-1723.

According to Matin (1972), "Perhaps the most elementary fact of visual space perception is that the spatial order of stimulus points in the environment remains correctly preserved in perception. Around this central fact has developed the general viewpoint that the visual perception of direction is mediated in the visual neurosensory pathway by a system of local signs that topographically maps locations of retinal stimuli into values of perceived direction".

Rather than directly attempting to measure the accuracy with which the absolute position of a local spatial feature can be estimated, it is usual to take an indirect approach. One such approach is to measure the just-noticeable *spatial difference* in the location(s) of two or more local spatial features e.g. by means of the vernier acuity procedure or the bisection acuity procedure (reviewed in Westheimer, 1979, 1981 and Morgan, 1991).

A recent theoretical attempt to model the encoding of positional information is a hybrid of the theory of local signs and spatial filter theory. According to this line of thought, small differences in the separation of closely separated spatial features are encoded in terms of the relative activity of the different spatial filters that are fed from the same spatial location, but for large separations between spatial features, local sign becomes important (Wilson, 1985, 1986, 1991; Klein and Levi, 1985). Another kind of spatial model — the

Watt and Morgan (1985) theory of spatial primitives — was developed from the theory of local signs via the centroid analysis of Westheimer and McKee (1977). A third kind of model postulates coincidence detectors that signal the simultaneous activation of widely separated receptive fields (Morgan and Regan, 1987).

A limitation of the several models just discussed, is that their primary purpose is to describe the processing of positional information about *luminance-defined* (LD) local features such as, for example, a bright line or a light-dark edge. In particular, the local spatial filters involved are the conventional spatial filters that respond to luminance-defined forms such as a Gabor patch. However, a local spatial feature in the retinal image can be rendered visible not only by luminance contrast, but also by any one of the following kinds of spatial contrast: color; motion; texture; disparity.

Physiologically plausible models of the detection of a texture-defined boundary typically involve several stages of processing subsequent to the local spatial filtering that can detect an LD boundary. For example, at an early stage in the processing of an orientation-texture-defined (OTD) boundary, the individual texture lines are detected by an array of spatial filters that respond to narrow luminance-defined targets. At a later stage of processing, the OTD boundary is detected by a nonlinear pooling of signals from early spatial filters fed from different regions of the visual field (Adelson & Bergen, 1985; Landy & Bergen, 1991; Bergen & Adelson, 1988; Fogel & Sagi, 1989; Sutter, Beck & Graham, 1989; Rubenstein & Sagi, 1990; Regan & Hong, 1995). It is, therefore, to be expected that an observer could more precisely locate a sharp high-contrast

LD boundary than an OTD boundary. But this would not be a fair comparison. A fair comparison would require that the spatial sampling frequencies of the LD and OTD targets were equated. A case in point is that aspect ratio discrimination threshold for an OTD rectangle is only 3.5% — not greatly different from 2.7% aspect ratio discrimination threshold for a (LD) rectangle of similar area whose spatial sampling is matched to that of the OTD rectangle (Regan *et al.*, 1996).

The aim of our project was to determine the precision with which positional information is encoded as a function of spatial sampling frequency for an OTD boundary, and to estimate the physiological limit. We used two methods for quantifying an observer's ability to discriminate the relative position of local features, namely vernier step acuity and bisection acuity. To compare positional acuity for OTD and LD boundaries, we repeated the experiments using an LD target whose spatial sampling frequency was matched to that of the OTD target.

Texture patterns were generated as follows. A computer (IBM PC clone) controlled two 16-bit digital to analogue converters (Cambridge Research Systems model D300) whose outputs drove the x- and y-axes of an electrostatically-driven large-screen (40 cm horizontal x 31 cm vertical) monitor with P31 phosphor (Hewlett-Packard model 1321A), thus allowing 65,536 x 65,536 screen locations to be addressed. A total of 1,536 short texture lines were drawn on the screen. The texture pattern covered a rectangular area that subtended 23 deg (vertical) x 15 deg (horizontal).

Technical details of texture pattern generation were as follows. The 65,536 x 65,536 screen locations were divided into a 48 x 32 rectangular array of square cells. Each cell had a side length [C in Fig. 1A] of 0.48 deg, and contained 512 x 512 locations. A line defined by two or more dots could be drawn inside each cell. In the present experiment we used three dots. The lines were not spaced regularly: the location of each line was individually jittered on a random basis. Had we used a regular rather than a spatially-jittered line pattern, vernier and bisection acuity thresholds would have had a lower limit equal to the distance between adjacent lines. We used the largest amplitude of jitter that did not cause overlap between lines. The center of each line was displaced from the center of its cell by distance d_V vertically and d_H horizontally [Fig. 1A]. The magnitude of d_V had an equal probability of falling at any value between zero and 0.3 of the cell's side length, and the displacement was randomly selected to be upwards or downwards. The magnitude of d_H similarly had an equal probability of falling at any value between zero and 0.3 of the cell's side length, and the displacement was randomly selected to be leftwards or rightwards. The magnitude and direction of the vertical and horizontal jitter displacements were determined by different random functions.

After calculating the jitter of every individual texture line, an imaginary vertical line was drawn at the center of the texture pattern. The line's location in the horizontal direction could be varied by one part in 65,536 of the width of the pattern, so that the line generally passed through cells rather than running along the boundaries between cells. For the OTD boundary there were two textures. For texture pattern 1, all texture lines whose centers fell to the left of

the imaginary vertical line had orientation θ_1, and all texture lines whose centers fell to the right of the imaginary vertical line had orientation θ_2. The two orientations θ_1 and θ_2 were symmetrical about the vertical. For texture pattern 2, θ_1 and θ_2 exchanged places. The magnitude of θ_1 and θ_2 could be varied from 0 deg to 180 deg. When the magnitude of $(\theta_2 - \theta_1)$ was less than 90 deg, orientation contrast (B) was equal to $(\theta_2 - \theta_1)$. When the magnitude of $(\theta_2 - \theta_1)$ was greater than 90 deg, B was equal to $[180 - (\theta_2 - \theta_1)]$ deg.

To prevent observers from using the sign or the orientation of an individual line(s) in a particular location on the pattern as a cue to the task each stimulus presented had an equal probability of being texture pattern 1 or texture pattern 2.

Luminance-defined (LD) boundaries were also used. For the LD boundary, all the texture lines had the same orientation and there were two luminance patterns. For luminance pattern 1, all texture lines whose centers fell to the left of the imaginary vertical line had luminance L_1, and all texture lines whose centers fell to the right of the imaginary vertical line had luminance L_2. For luminance pattern 2, L_1 and L_2 exchanged places. Luminance contrast was defined as equal to $100(L_1 - L_2)/(L_1 + L_2)$.

To prevent observers from using the sign of the luminance of an individual line(s) in a particular location in the pattern as a cue to the task each stimulus presented had an equal probability of being luminance pattern 1 or luminance pattern 2.

In all the experiments described below the texture pattern was displayed only during a presentation of duration 200 msec, a value short enough to ensure that observers could not scan the pattern by means of eye movements. The positional jitter of the texture lines were re-computed for every presentation.

We measured vernier step threshold for an OTD boundary using targets similar to that illustrated in Fig. 1(B). Spatial sampling frequency and line length were varied simultaneously by varying viewing distance from 45 to 1280 cm. Filled symbols in Fig. 2(A) show that vernier step sensitivity (i.e. reciprocal of vernier threshold) for the LD boundary was proportional to the number of lines per deg over a wide range of spatial sampling frequencies.

Over the range of sampling frequencies between 2 and 20 samples/deg, vernier step sensitivity was not greatly less for the OTD boundary than for the LD boundary [mean ratio were 2.5 (SE = 0.4): 1 and 4.4 (SE = 0.8): 1 for observers 1 and 3 respectively.

However, as sampling frequency grew appreciably greater than 20 samples/deg, vernier step sensitivity fell steeply for the OTD boundary. The ratio between vernier step sensitivities for LD and OTD boundaries was much larger than for sampling frequencies below 20 samples /deg. For example, at a sampling frequency of 30 samples/deg, ratios were 132:1 and 105:1 for observers 1 and 3 respectively).

Fig. 2(B) shows that results were similar for bisection acuity. Over the range of sampling frequencies between 2 and 20 samples/deg, bisection acuity sensitivity was only slightly lower for the OTD boundary than the LD boundary

[mean ratios were 1.3 (SE=0.1):1 and 1.5 (SE=0.2):1 for observers 1 and 3 respectively].

As was the case for vernier step acuity, when spatial sampling frequency was appreciably greater than 20 samples/deg the data points departed from the line (open circles in Fig. 2B).

For sampling frequencies greater than 20 samples/deg, bisection acuity sensitivity fell sharply. The ratio between bisection acuity sensitivities for LD and OTD boundaries was much larger for sampling frequencies greater than 20 samples/deg than for lower sampling frequencies. For example, at a sampling frequency of 30 samples/deg, ratios were 24:1 and 33:1 for observers 1 and 3 respectively).

We propose that the lowest values of vernier step acuity threshold (2.3 and 2.4 min arc for observers 1 and 3, respectively), and the lowest values of bisection acuity threshold (1.7 & 1..9 min arc for observer 1 and 3 respectively) approach the physiological lower limits for an OTD boundary. We suggest that these physiological limits reflect a balance between two opposing tendencies: increasing the spatial sampling frequency tends to lower the positional acuity thresholds; on the other hand, reducing the length of the texture lines below approximately 1 min arc (this occurred at a sampling rate of 20 samples/deg in the present study) degrades the discrimination of line orientation and the visibility of an OTD boundary.

Rather than comparing positional acuities for OTD and LD boundaries that are matched for spatial sampling frequency, it is also of interest to compare the physiological limits of positional acuities for the two kinds of boundary. For

sharp-edged high contrast LD boundaries whose spatial sampling frequency is very high, vernier step acuity can be as low as 2 to 5 sec arc and bisection acuity can be as low as 1 to 5 sec arc. Our proposal that the corresponding physiological limits for OTD boundaries are close to 2.3 to 2.4 min arc and 1.7 to 1.9 min arc implies that, at the physiological limits, the ratios between thresholds for OTD and LD boundaries are about 80:1 for vernier step acuity and 40:1 for bisection acuity, presumably because of the spatial pooling that precedes detection of an OTD boundary.

Finally, we investigated acuity for boundaries defined by a combination of texture contrast and luminance contrast. We interleaved 5 measurements of vernier acuity threshold for each of the following three conditions: (1) $\beta = 70$ deg, C = 20%; (2) $\beta = 70$ deg, C = 0%; (3) $\beta = 0$ deg, C = 20%. Vernier acuity thresholds for the three conditions are shown in Fig. 3. Black bars are for condition 1, white bars are for condition 2 and grey bars are for condition 3. It is evident to visual inspection that vernier threshold was lowest for condition 1, intermediate for condition 2 and highest for condition 3. For subject 1, two tailed t-tests revealed a significant difference between (luminance + texture) versus texture alone ($t = 3.38$, $p < 0.001$, $dF = 8$) and (luminance + texture) versus luminance alone ($t = 4.83$, $p < 0.001$, $dF = 8$). Corresponding statistics for observers 2 and 3 were as follows. Observer 2: $t = 3.3$, $p < 0.001$, $dF = 8$ and $t = 7.65$, $p < 0.001$, $dF = 8$. Observer 3: $t = 2.72$, $p < 0.05$, $dF = 8$ and $t = 13.4$, $p < 0.001$, $dF = 8$.

We conclude that observers can combine positional information carried by texture contrast and with positional information carried by luminance contrast. Figure 3 indicates that the combination rule is not "winner take all". Nor is there evidence of marked nonlinear facilitation. Our findings are consistent with probability summation between independent channels. Our findings complement those of Rivest and Cavanagh (1996) in showing that, when the special advantage of high resolution for solid high-contrast targets is removed, luminance contrast does not have an overriding role in encoding boundary location

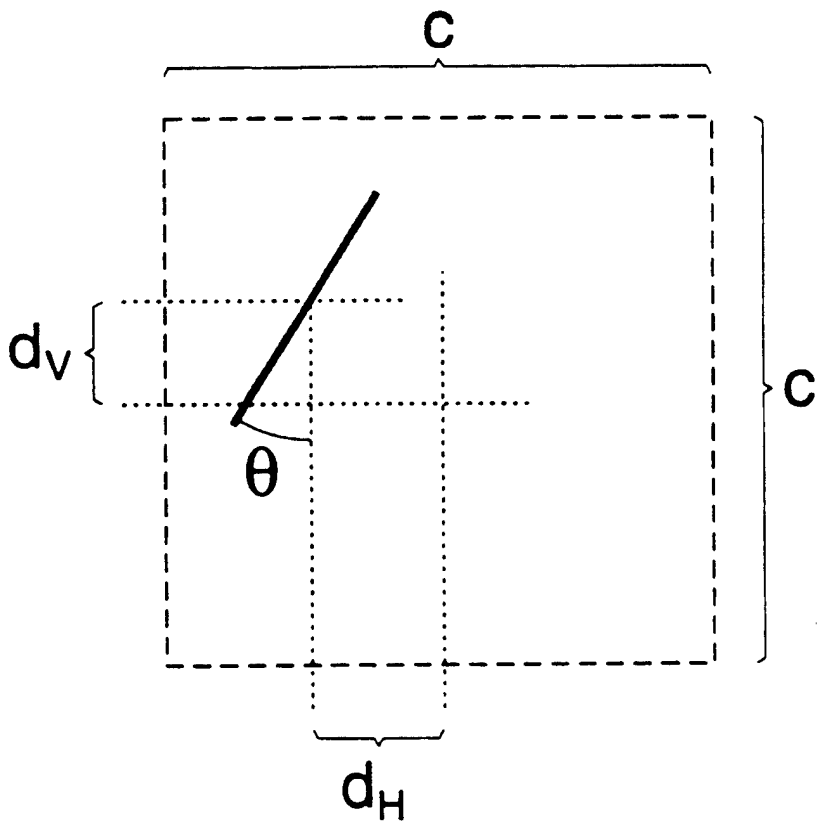

Figure 1. A: The texture pattern was divided into 1536 imaginary cells, each of side length c deg. A texture of length 0.3c was drawn within each cell. The center of each line was displaced from the center of the cell in a random direction. The magnitudes of the displacements d_V and d_H ranged from zero to 0.3c. B: Texture–defined vernier step target.

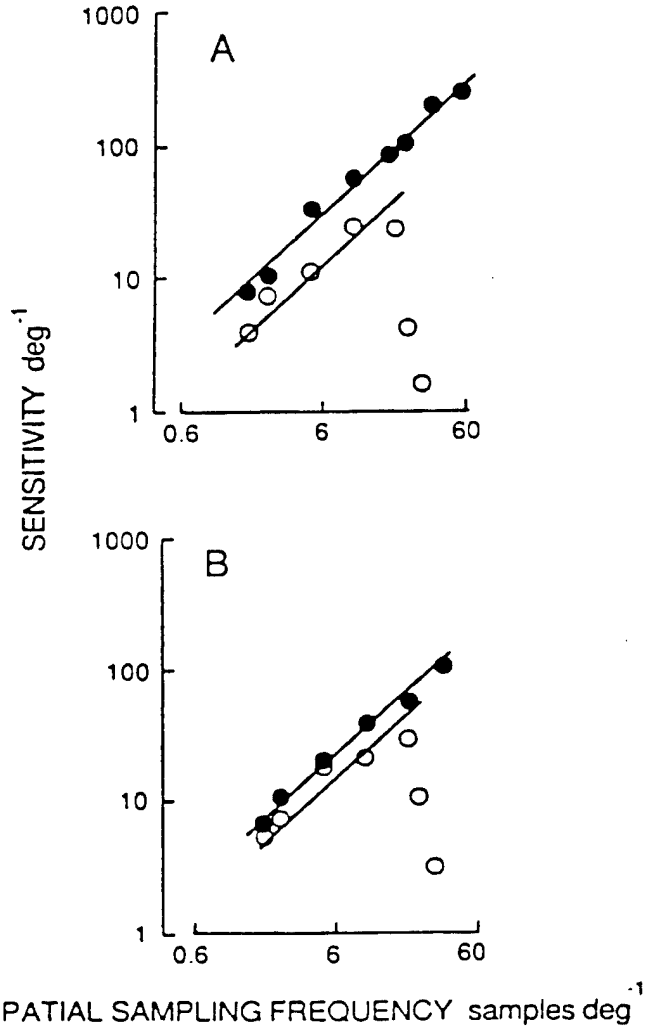

Figure 2. A: Vernier step sensitivity for luminance–defined (filled symbols) and texture–defined (open symbols) boundaries plotted versus the spatial sampling frequency (i.e. number of texture lines per deg of vision (angle). B: Bisection sensitivity plotted versus sampling frequency. Other details as for A. Vernier step sensitivity is the reciprocal of vernier step threshold, and bisection sensitivity is the reciprocal of bisection acuity.

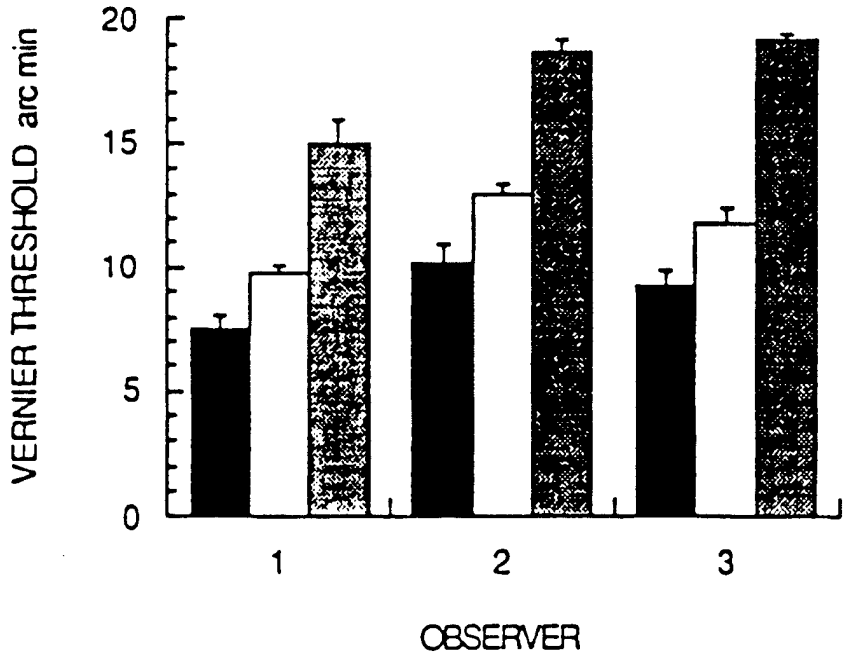

Figure 3. Vernier step acuity thresholds for boundaries defined by combinations of orientation contrast (β) and luminance contrast (C). Black bars: β =70 deg, C=20%. White bars: β =70 deg, C=0%. Gray bars: β =0 deg, C=20%.

2.1. (b) Spatial frequency discriminations and detection characteristics for gratings defined by orientations texture.

Long-Term Aims 1.1.2a, 1.1.2d; Specific Aims 1.2.1b.

This project is completed and a paper has been published. Gray, R. & Regan, D. (1997). Spatial frequency discrimination and detection characteristics for gratings defined by orientation texture. Vision Research, 38, 2601-2617.

Fig. 4 shows an orientation-texture-defined grating of high orientation contrast. Fig. 5 shows how line orientation varied across the grating. The grating's orientation contrast (β deg) was equal to Δθ in Fig. 5, where Δθ was the

maximum difference in line orientation across one cycle of the grating. Starting phase (α_s deg in Fig. 5) was set randomly before every presentation.

In control experiments we established the minimum number of texture lines per degree of visual angle (i.e. the minimum spatial sampling frequency) required to ensure that spatial frequency discrimination threshold was not limited by spatial sampling frequency. Our starting point was to vary randomly the total number of texture lines in the display on a trial-to-trial basis. This ensured that any aliasing patterns could provide no reliable cue to the grating's spatial frequency. We also wished to ensure that, if any variation of perceived contrast was produced by changing spatial frequency, this variation provided no reliable cue to spatial frequency. To achieve these aims we used the following experimental design. The stimulus set consisted of six values of spatial frequency, six values of orientation contrast, and six values of the number of texture lines per deg, giving 216 stimuli, each of which was presented once during any given run. Spatial frequency and orientation contrast had zero correlations. Each trial consisted of a single short (200 msec) presentations. Observer were instructed to press one of two buttons depending on whether the grating's spatial frequency was higher or lower than the mean of the set of 216 stimuli.

Similar measurements were carried out for luminance-defined (LD) gratings.

Fig. 6(A) - (C) demonstrates the method and shows that the observer based responses on the task-relevant variable (i.e. spatial frequency), and ignored orientation contrast and number of lines per deg.

Using this method we measured spatial frequency discrimination threshold as a function of spatial frequency with a spatial sampling frequency of 2.3 lines/deg. Because of our "sampling jitter" trick, the task was impossible when the number of lines per grating cycle fell to two, but threshold had already started to rise when the number of lines per grating cycle had fallen to six. This was also the case for sampling frequencies different from 2.3 lines/deg. We concluded that threshold would not be limited by sampling frequency provided that the number of lines per grating cycle did not fall below six.

We then addressed the problem that, if we wished to use progressively higher spatial frequencies, the number of lines/deg would have to be progressively increased, and if line overlap were to be avoided line length would have to be progressively reduced. Clearly, this could not go on indefinitely, because if the lines became too short line orientation discrimination would fail so that the grating would not be visible at all.

To elucidate this point, we measured spatial frequency discriminations threshold [ordinate in Fig. 7(A) & (B)] as a function of the number of lines per grating cycle [lower abscissa in Fig. 7(A) & (B)]. Spatial sampling frequency and line length were varied in the yoked manner characteristic of a change in viewing distance. Open circles show data for OTD gratings. Discrimination threshold fell steeply as the number of spatial samples per grating cycle was progressively increased from 2. Over this range, line length decreased from 12

to 4 - 6 min arc. However, as the number of samples per grating cycle increased beyond 17 (and at the same time line length grew progressively shorter than 1.5 min arc), spatial frequency discriminations threshold started to rise until discrimination eventually became impossible. The minimum threshold was 5.6 in Fig. 6 (A) and 5.0% in Fig. 6(B), and the length of the texture lines was approximately 2.5 min arc at minimum threshold.

In a separate experiment we showed that, with texture line length held constant, discrimination threshold for an OTD grating was approximately independent of spatial sampling frequency until the number of lines per grating cycle fell to approximately 6, after which threshold rose steeply. We also showed that, with the spatial sampling frequency held constant at 6 lines per grating cycle, discrimination threshold was little affected by line length until line length fell below approx. 1.2 min arc. Threshold then rose very steeply.

We proposed that the minimum threshold for OTD gratings in Fig. 7(A) & (B) reflected a balance between two opposing tendencies. Increasing the number of lines per grating cycle beyond about six causes discrimination threshold to asymptote to a minimum value. However, when the associated reduction of line length causes line length to fall below 1.2 min arc, discrimination is degraded.

We propose that the minimum threshold in Fig. 7(A) & (B) approaches the physiologically-determined lower limit for OTD gratings.

The procedure just described was repeated over a range of spatial frequencies to give the discrimination curve shown as open circles in Fig. 8(A)

& (B). For comparison, filled circles show the discrimination curve for LD gratings of matched spatial sampling frequency.

Spatial frequency discrimination thresholds are the same for OTD and LD gratings over a range of low spatial frequencies (0.07c/deg to 0.3c/deg). Our interpretation is that, at low spatial frequencies, the ability to analyze the spatial frequency content of the visual scene is the same for OTD form and LD form. Spatial frequency discrimination for OTD grating does not fail until spatial frequency is greater than at least 7c/deg. We propose a model of a neural mechanism sensitive to OTD form that can account for our findings, reported previously, on spatial frequency discrimination, orientation discrimination, and width discrimination for OTD form (see below).

A paper was submitted to *Vision Research* but returned with a request that we compare our findings with those of Kingdom et al. (1994) *Vision Research* (1994), 35, 79-91. Although the study of Kingdom et al. was confined to OTD grating detection, their conclusions are not consistent with our findings on OTD grating discrimination. They reported that: (a) sensitivity peaks at 0.06-0.2c/deg and falls off at lower and higher frequencies; the curve shifts bodily when viewing distance is increased, a finding they interpreted to imply that sensitivity is set by the number of cycles per cm across the display rather than by the retinal image. In brief, we confirmed their findings, but showed their conclusions to be flawed. In particular: sensitivity is determined by the spatial frequency of the retinal image rather than by the spatial frequency of the display; the attenuation they reported at low spatial frequencies was caused by using too few cycles (as low as one complete cycle); the attenuation they

reported at spatial frequencies above 0.2 c/deg was caused by undersampling. When we attended to these points, we obtained a very different curve for OTD gratings: flat to about 3.0c/deg, with an OTD grating acuity beyond 13.0c/deg.

Fig. 9(A) & (B) show our grating detection characteristics for OTD (filled circles and LD (open circles) gratings.

The well-known contrast sensitivity curve for LD gratings is widely regarded as representing the upper envelope of the sensitivities of many spatial filters that analyze at different spatial scales (reviewed in Atkinson, Braddick & Campbell, 1978). One suggestion as to how this is achieved is that local LD spatial information is passed through an array of parallel spatial filters which prefer LD targets of different widths. The receptive field profile of each filter consist of an elongated excitatory center surrounded by elongated inhibitory flanks, often modeled as a "Mexican hat" profile (reviewed in Wilson, 1991).

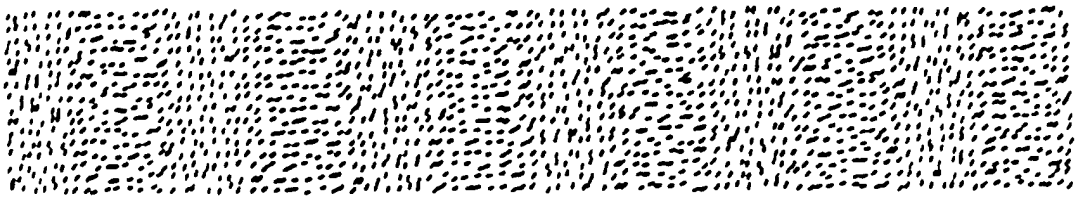

Figure 4. Texture–defined grating.

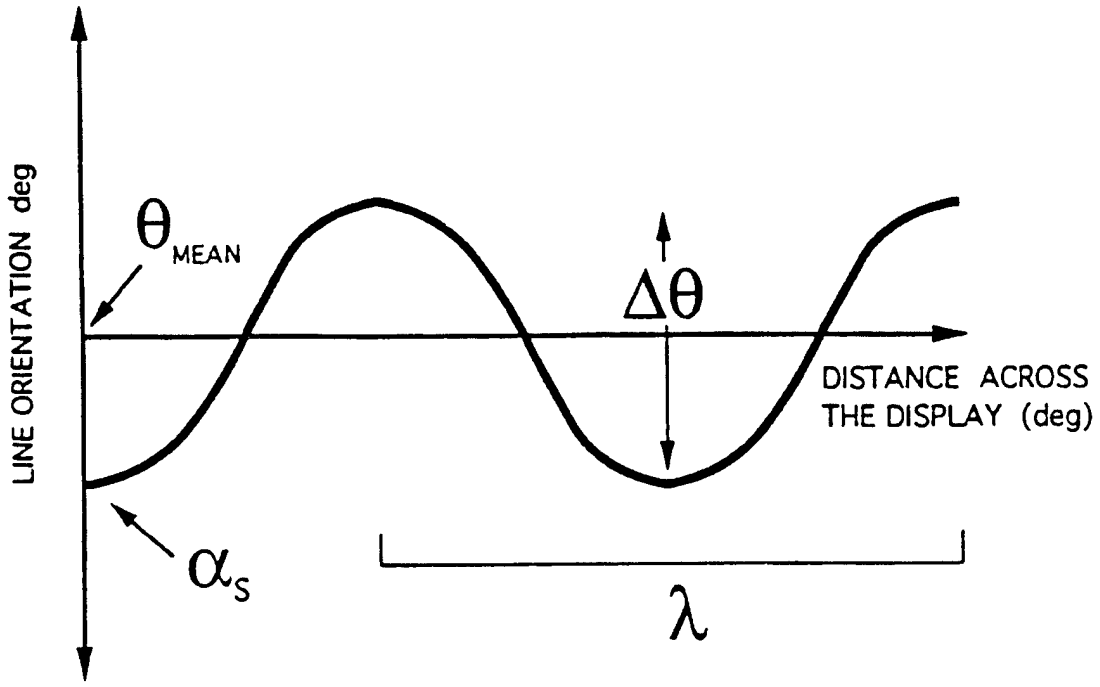

Figure 5. Variation of texture line orientation across a texture–defined grating.

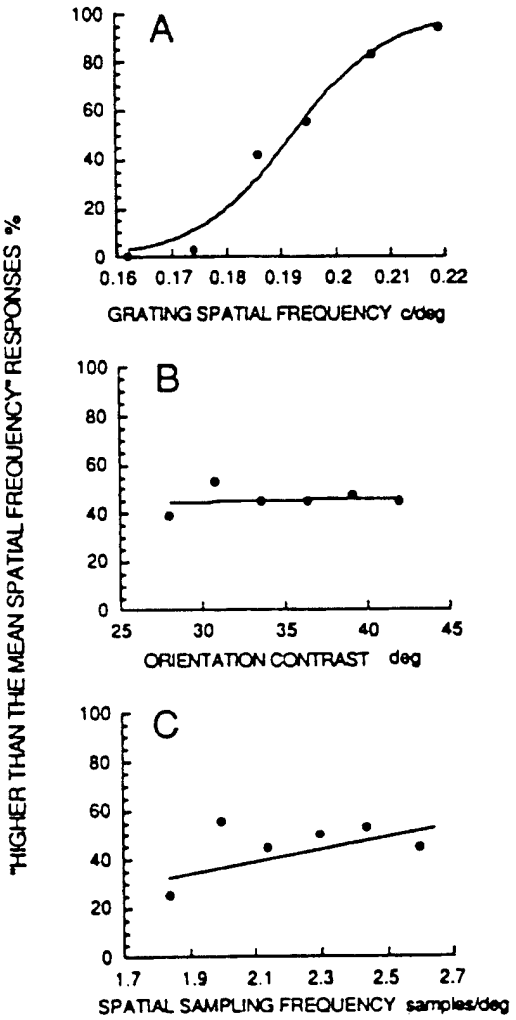

Figure 6. Spatial frequency discrimination for a grating defined by orientation contrast. The percentage of "higher spatial frequency than the mean" responses is plotted versus the spatial frequency of the test grating (the task–relevent variable) in panel A, versus the grating's orientation contrast (task–irrelevent variable #1) in panel B, and versus the number of spatial samples per deg (task–irrelvent variable #2) in panel C. The grating's mean spatial frequency was 0.2c/deg. Mean orientation contrast was 35 deg.

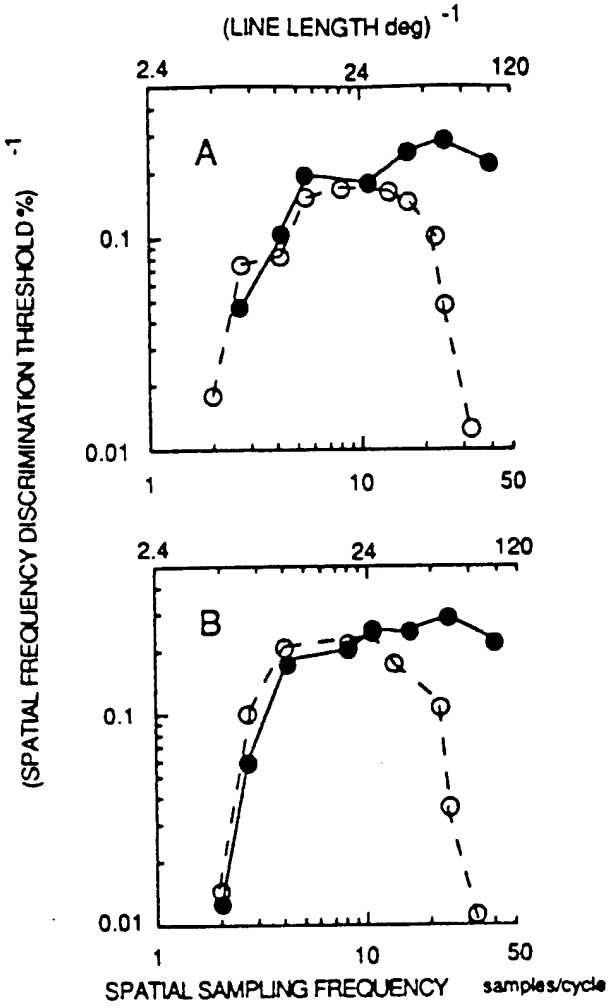

Figure 7. Effect of simultaneous variation of the number of spatial samples per grating cycle and line length on spatial frequency discrimination. Open circles: texture–defined grating. Filled circles: luminance–defined grating. The reciprocal of spatial frequency discrimination is plotted (ordinate) while the number of spatial samples per grating cycle and line length were varied in the yoked manner characteristic of a change in viewing distance (abscissae). A: observer 1. B: observer 2.

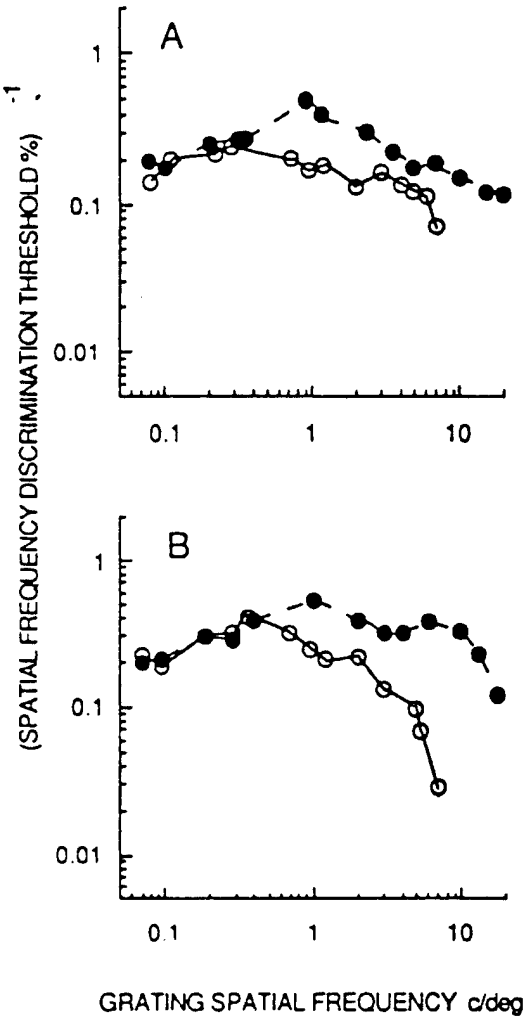

Figure 8. The reciprocal of spatial frequency discrimination threshold is plotted versus grating spatial frequency. Thresholds for grating with six or more spatial samples per grating cycle are signified by open circles (texture–defined gratings) and filled circles (luminance–defined gratings). A: observer 1. B: observer 2.

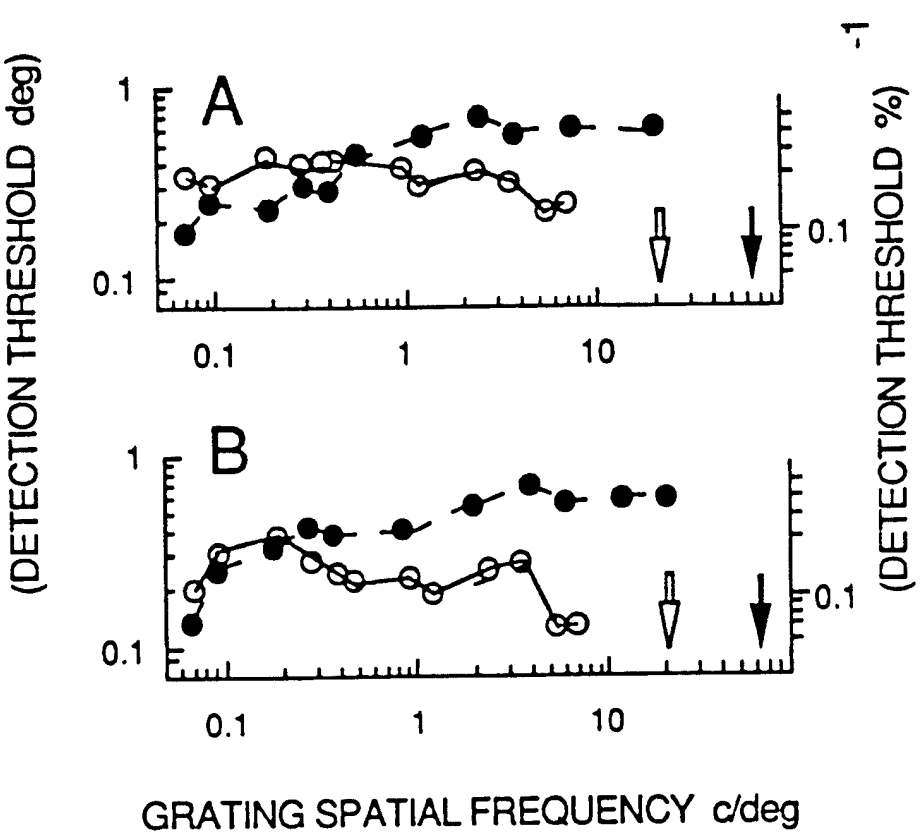

Figure 9. The reciprocal of grating detection threshold, for texture-defined gratings (open symbols, left ordinate) and for luminance-defined gratings (solid symbols, right ordinate), was plotted versus grating spatial frequency. Detection thresholds for gratings with six or more spatial samples per cycle are signified with open circles (texture-defined gratings) and filled circles (luminance-defined gratings). The number of spatial samples per grating cycle fell to two at a spatial frequency of 21 c/deg (open arrows) for texture-defined-gratings and at 66 c/deg (solid arrow) for luminance-defined-gratings. A: observer 1. B: observer 2.

Within this context, our finding that detection threshold is approximately constant over a range of spatial frequencies from 0.07 to 3.6 cycles/deg can be understood if orientation contrast information is passed through an array of parallel spatial filters which prefer OTD targets of different widths and that over a range of bar widths from 7 deg to 0.14 deg, any given bar is detected when the total change of orientation within the receptive field tuned to the

width of that particular bar exceeds some fixed threshold (about 2 to 3 deg for observer 1, 3.5 to 6 deg for observer 2). This implies that the orientation gradient at detection threshold is inversely proportional to receptive field width over the range of receptive fields that prefer bars whose widths lie between 7 deg and 0.14 deg.

It is well known that the visual detection of LD gratings does not fail until 35 to 50 cycles/deg. Our finding that the visual detection of OTD gratings fails at a considerably lower spatial frequency can be understood in terms of multi stage models of the detection of OTD form. According to several models of this kind, the first stage of processing OTD form consists of a parallel array of LD form filters, each tuned to the orientation of a particular texture line. Later stages of processing involve spatial integration. According to this idea, it is the spatial integration stage that is responsible for the early high-frequency rolloff in the OTD grating detection characteristic.

Spatial frequency discrimination threshold can be regarded as a measure of sensitivity to differences in the spatial scale of scene content. Our present findings indicate that at low spatial frequencies human ability to analyze the spatial frequency content of the visual scene is approximately the same for spatial features rendered visible by texture contrast and for features rendered visible by luminance contrast. As spatial frequency is increased, sensitivity to differences in spatial scale grows progressively less for OTD form relative to LD form but, as already mentioned, the ability to discriminate different spatial frequencies for OTD gratings does not fail entirely until beyond 7 cycles/deg.

It is well known that spatial frequency discrimination threshold for LD gratings is considerably less than the spatial frequency tuning bandwidth of cortical neurons in primate. One proposed explanation for this conflict is that discrimination threshold is determined by the relative activity of neurons that prefer different spatial frequencies (Campbell, Nachmias & Jukes, 1970; Regan, 1982; Regan & Beverley, 1983; Wilson & Regan, 1984). The finding that spatial frequency discrimination threshold for LD gratings saturates at moderate contrasts can also be explained in terms of this proposal (Regan et al., 1982). Our present finding that, over a wide range of spatial frequencies, spatial frequency discrimination threshold for OTD gratings is as low as for an LD gratings and, in addition, is independent of orientation contrast might also be understood if spatial frequency discrimination threshold for OTD gratings is determined by the relative activation of multiple receptive fields that prefer OTD targets of different widths.

Our findings can be explained in terms of the hypothetical double-opponent receptive field depicted in Fig. 10. When the excitatory part of the receptive field (shown by the dashed circle in Fig. 10(A) & (B) is stimulated by short lines of the preferred orientation, and the inhibitory surround is simultaneously stimulated by the lines of the same orientation the net excitation is zero. If the lines falling on the excitatory region do not change orientation while the lines falling on the inhibitory region are slowly rotated, the net excitation progressively increases. Excitation reaches a maximum in the situation depicted in Fig. 10(B). Suppose now that we sum many receptive fields of the kind depicted in Fig. 10(A) & (B), all of which are driven from the

same receptive field locus, but which prefer different line orientations. Such a double-opponent receptive field will be excited by lines of any arbitrary orientation $\underline{\theta}_1$, provided that the lines that fall on the excitatory region all have orientation $\underline{\theta}_2$, where $\underline{\theta}_2 \neq \underline{\theta}_1$.

Suppose that, as illustrated in Fig. 10(C), we sum the outputs of several such double-opponent receptive fields that lie along a straight line in retinal coordinates (dashed circles). The resulting elongated receptive field will have the line orientation sensitivity profile shown by the continuous line in Fig. 10(C). It will be strongly excited by an isolated OTD bar or by the bars of the OTD gratings illustrated in Fig. 11(A), (C) & (D), provided that the bar or bars are matched to the width and orientation of the excitatory region of the receptive field.

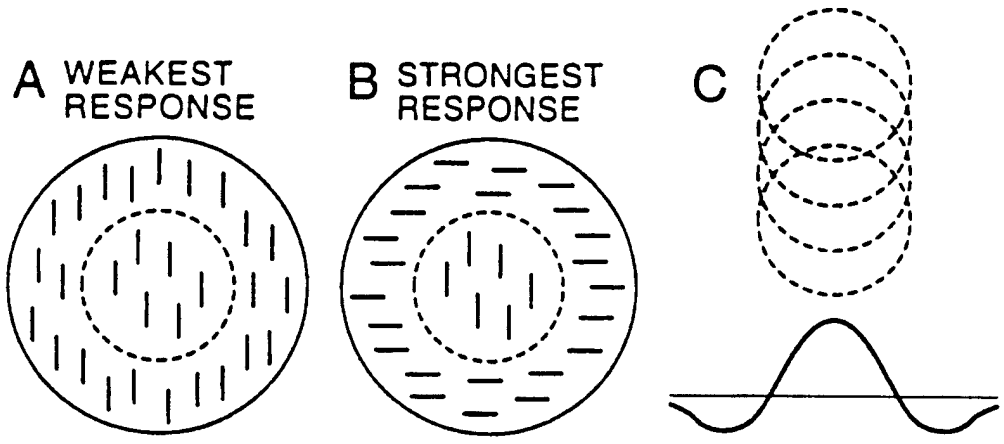

Figure 10. Model of an orientation - and size - tuned filter for OTD form. A & B: The double-opponent receptive field consists of an excitatory center (dashed circle) with an inhibitory surround. Texture lines are shown with the preferred orientation for the excitatory regions. C: The orientation-tuned filter is built by summing the outputs of many such receptive fields whose centers fall along a straight line so as to give an elongated receptive field whose profile is shown by the continuous line.

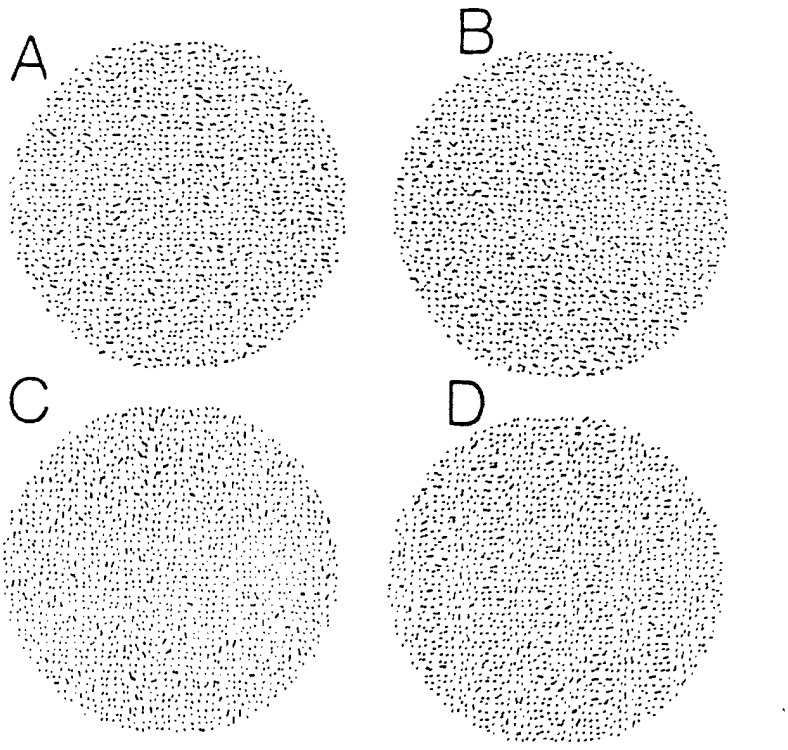

Figure 11. Photographs of texture patterns. A: Vertical orientation-texture-defined (OTD) grating with maximum possible orientation contrast (90 deg) and mean line orientation 0 deg. B: Scatter pattern matched to the grating shown in panel A. Each line in the scatter pattern corresponds to a line in the grating, and vice versa, but the lines are ordered in grating and randomly-placed in the scatter pattern. C: Mean line orientation 45 deg, orientation contrast 60 deg. C: Mean line orientation 90 deg, orientation contrast 60 deg. Angles 0-180 deg clockwise of vertical are taken as positive, and angles 0-180 deg anticlockwise of vertical are taken as negative.

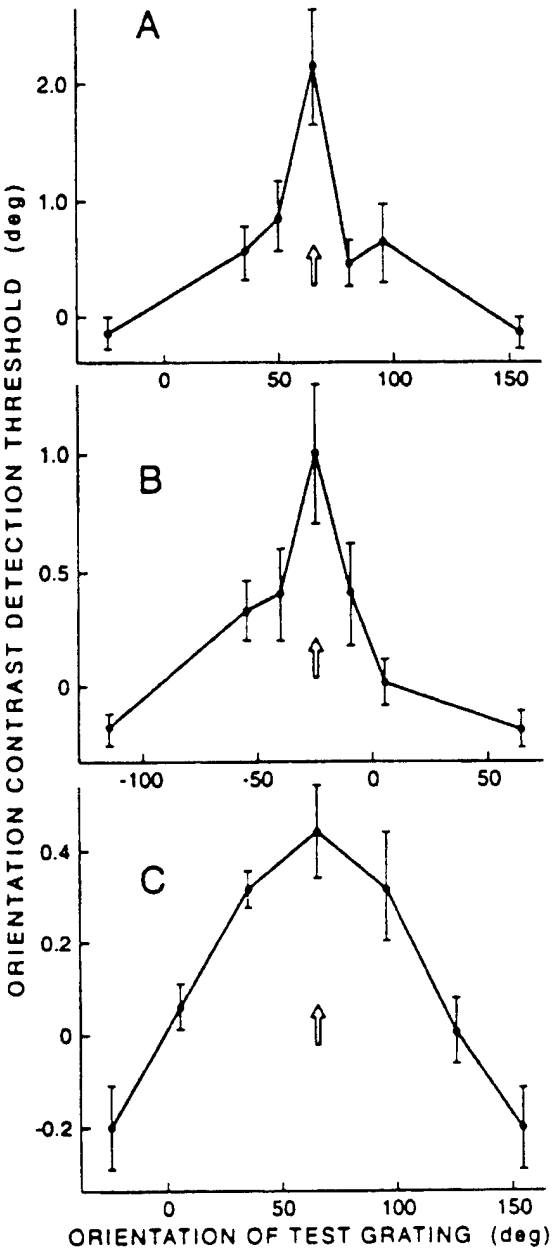

Figure 12. Grating detection threshold elevations produced by adapting to an orientation-texture-defined (OTD) grating were plotted versus the orientation of the test OTD grating. Arrows indicate the orientation of the adapting grating. A, B: observer 1. C: Observer 2. Vertical bars indicate ±1 standard error.

2.1 (c) Orientation-tuned spatial filters for texture-defined form

Long-Term Aims 1.1.1 (a), 1.1.2 (a), (d); Specific Aims 1.2.3. This project is completed, and a paper has been published. Kwan, L. & Regan, D. (1998). Orientation - tuned spatial filters for texture - defined form. Vision Research, 38, 3849-3855.

The purpose of this study was to test the model shown in Fig. 10. We used a selective adaptation approach analogous to the classical Blakemore & Campbell study, except that we used OTD gratings instead of LD gratings

The rationale was as follows. Two adapting patterns were used. One was an OTD grating; the other was used to measure baseline thresholds. The adapting grating had the highest possible orientation contrast of 90 deg [e.g. Figure 11(A)]. In total there were eight possible spatial phases of the adapting grating, spaced at uniform intervals from zero to 360 deg. During the adaptation and "refresh adaptation" periods, the phase of the adapting grating changed abruptly every 0.5 sec to a different value selected randomly from seven possibilities.

Baselines were measured by replacing the adapting grating with a scatter pattern matched to the particular adapting grating. Fig. 11 (B) shows a scatter pattern matched to the grating shown in Fig. 11 (A). The scatter pattern in Fig. 11 (B) contains every one of the lines in the Fig. 11 (A) grating. The only difference between Fig. 11(A) and (B) is that the individual lines are scattered randomly within the pattern in Fig. 11(B) rather than being ordered as in Fig. 11(A). For each adapting grating there were eight different scatter patterns. During the adapting and refresh periods the scatter pattern changed abruptly every 0.5 sec to a random selection of one of the other seven patterns.

The only difference between the adapting grating and the scatter pattern was the ordered vs. random spatial arrangement of the texture lines. Therefore, any difference in the grating detection thresholds measured after adapting to the two patterns can be attributed to the ordered vs. random arrangement of the texture lines, i.e. to the presence of the OTD grating. Because both grating and scatter patterns were changed every 0.5 sec, adaptation caused by the texture lines themselves would be the same in both conditions.

Our findings are shown in Fig. 12(A)-(C) where of postadaptation threshold elevations are plotted versus the orientation of the test grating. In each case, the orientation of the adapting grating is arrowed. In all cases, threshold elevation was largest for a test grating parallel to the adapting grating. Threshold elevation for test gratings parallel to the adapting grating were considerably and significantly higher than thresholds for test gratings perpendicular to the adapting gratings. In every experimental condition, threshold for a test grating perpendicular to the adapting grating threshold elevation was not significantly different from zero.

We conclude that adapting to an OTD grating produces an orientation-tuned detection threshold elevation for subsequently-presented OTD test gratings. We conclude that the human visual system contains orientation-tuned filters sensitive to OTD form. We have no evidence that adapting to an OTD grating reduces detection threshold for a test grating perpendicular to the adapting grating.

Next we aimed to find out how the sensitivity of the filter that responded most strongly to an OTD grating depended on (a) the orientation of the grating,

and (b) the relations between the orientation of the grating and the mean orientation of the texture lines.

The appearance of some of the test gratings is illustrated in Fig. 11(A), (C) & (D), where the OTD gratings are all vertical, but in Fig. 11(A) the mean line orientation is horizontal (and orientation contrast is 90 deg), while in Fig. 11(C) & (D) the mean line orientations are, respectively, vertical and 45 deg (and orientation contrast has been reduced to 60 deg).

Grating detection threshold was measured for four different grating orientations (0 deg, 45 deg, 90 deg & 135 deg) while the mean orientation of the texture lines was held constant at 0 deg. This procedure was then repeated for mean line orientations of 45 deg, 90 deg and 135 deg.

Thresholds for all four observers and all 16 conditions were analyzed by repeated measures analysis of variance (ANOVA). Neither grating angle nor line angle had any significant effect. In particular, there was no significant difference in detection thresholds when texture lines were parallel to the grating and when they were perpendicular to the grating.

Our proposed explanation for the findings shown in Fig. 12 is as follows: (a) the human visual system contains neural filters each of which has the elongated double-opponent receptive field just described; (b) each retinal location is served by several such filters that prefer different OTD bars of different orientations.

Orientation discrimination threshold for an OTD bar is almost as low as for a luminance-defined bar of matched spatial sampling (0.6 deg compared with 0.4 deg), and this is considerably less than the orientation-tuning

bandwidths in Fig. 12 (A) - (C) or the orientation-tuning bandwidth of the most sharply-selective cortical neurons. A proposed explanation for this conflict is that orientation discrimination threshold is determined by the relative activity within a population of orientation-tuned filters for OTD form (Regan, 1995). This idea can be framed in either opponent-process or line-element format. The organization depicted in Fig. 10(C) would also explain why contrast detection threshold for an OTD bar was the same whether the mean orientation of the lines inside the bar were parallel or perpendicular to the bar (Regan, 1995).

The large elongated double-opponent receptive fields that, we suppose, detects the 0.48 c/deg grating shown in Fig. 11(A) and the 5.0 x 1.4 deg OTD bar used in a previous study to measure orientation discrimination threshold (Regan, 1995) achieves image segregation by grouping for similarity ("regional binding"). For example, in the case of the bar it is sensitive to the fact that line orientation was constant within a 5.0 x 1.4 deg area and different outside that area. There are, however, OTD targets that would not be detected by an OTD filter that was matched to the size of the target. Nothdurft (1994) has provided an illustration of such a target in the form of a clearly-visible OTD square, and has pointed out his square target is rendered visible by locally-increased orientation contrast gradient across the boundaries of the target. Such a boundary would be highlighted by spatially-opponent receptive fields whose excitatory region was much smaller than the target. Depending on the kind of lateral interaction within the receptive field, small receptive fields of this kind translate the orientation contrast gradient across a boundary into either a high-

intensity line on a low intensity background or into a low-intensity line on a high-intensity background [as was the case for the double-opponent receptive field model described by Regan and Hong (1995)].

2.2 Visual Processing of Time To Collision

Relevance: The relevance of this line of research is as follows: collision avoidance in both fixed-wing and rotary-wing aviation; the design of binocular and monocular flight simulators and, in particular, transfer of training in collision avoidance.

2.2 (a) Estimates of time to collision with an approaching object based on binocular information, monocular information and combined binocular and monocular information

Long-Term Aims 1.1.1 (a), 1.1.1 (c), 1.1.2 (a), (c), (e); Specific Aims 1.2.6, 1.2.7, 1.2.8. The project is completed and a paper has been published. Gray, R. & Regan, D. (1998). Accuracy of estimating time to collision using binocular and monocular information. Vision Research, 38, 499-512.

Hoyle (1957) showed that the time to collision (T) with an approaching rigid spherical object is given by the equation

$$T \approx \theta/(d\theta/dt) \quad \text{---------- (1)}$$

We have developed a method for measuring precisely errors in an observer's estimates of discriminating trial-to-trial variations of time to collision to estimating absolute time to collision. In a study reported by Gray & Regan (1997) each trial consisted of one 0.7 sec presentation of the approaching

target. At the designated time to collision, some time after the target had disappeared, there was a brief auditory tone whose timing could be set to an accuracy of 0.001 sec. The observer was instructed to press one of two buttons depending on whether the click occurred before the simulated approaching sphere would have hit the head. The value of $\theta/(d\theta/dt)$ was varied by the computer that controlled the experiment according to the observer's previous button presses. We used the staircase method described by Levitt (1971). Three designated times to collision (1.69, 2.09 & 2.72 sec) were combined with three starting sizes (0.41, 0.68 & 0.9 deg) to give a total of nine interleaved staircases.

The solid bars in Fig. 15 show the mean percentage differences between the designated and estimated times to collision. Confirming previous reports (Schiff & Detwiler, 1979; Cavallo & Laurent, 1988), all observers consistently underestimated time to collision. Errors ranged from 2.0 to 12%. On the basis of these data plus the results of stepwise regression analysis we concluded that, provided the target is sufficiently large, observers can make accurate estimates of time to collision on the basis of the $\theta/(d\theta/dt)$ ratio alone, while ignoring simultaneous trial-to-trial variations in target size, rate of expansion and total change of size.

It is easy to see that judgements of time to collision based on the ratio $\theta/(d\theta/dt)$ will fail when the angular subtense of the approaching object is very small, because the rate of angular expansion would be undetectable. A less obvious point is expressed by the theoretical equation (2)

$$\frac{(d\theta / dt)}{(d\delta / dt)} \approx \frac{2S}{I} \quad \text{----------} \quad (2)$$

where, as illustrated in Fig. 2(A) & (B), $\theta/(d\theta/dt)$ is the rate of increase of the angular subtense of the approaching object, $d\delta/dt$ is its rate of change of binocular disparity, 2s is the linear width of the object (expressed, for example, in cm), and I is the interpupillary separation of the observer's eyes (Regan & Beverly, 1979). In words: the ratio between the monocular ($d\theta/dt$) and binocular ($d\delta/dt$) correlates of motion in depth depend on the approaching object's linear width (rather than angular subtense) independently of viewing distance.

We explored this point experimentally using a stimulus set that comprised 64 different combinations of time to collision [i.e. $\theta/(d\theta/dt)$], rate of expansion ($d\theta/dt$), change of size during a presentation ($\Delta\theta$), presentation duration and starting size. Observers were instructed to signal whether time to collision was shorter than the mean of the stimulus set. Filled and open circles in Fig. 14(A) are far targets of mean starting size 0.7 deg and 0.03 deg respectively. Fig 14(A) shows that discrimination threshold was considerably lower for the large target than for the smaller target. The difference between the two sets of data was, however, not merely quantitative. By subjecting the response data to stepwise regression analysis, it was found that, for the larger target size, observers based their responses on the task-relevant variables. In particular the ratio $\theta/(d\theta/dt)$ accounted for a high proportion of the variance (R^2 ranged from 0.72 to 0.80 for our four observers) and none of the other

variables entered ($d\theta/dt$, $\Delta\theta$, duration, starting size) accounted for a significant amount of variance. On the other hand, for the smaller target the ratio $\theta/(d\theta/dt)$ accounted for only a small proportion of variance (R^2 ranged for 0.15 to 0.42 for the four observers), and for two observers a task-irrelevant variable accounted for most variance. We concluded that monocular information does not provide a reliable basis for either discriminating variations in time to collision nor estimating its absolute value when object size is small. This does not mean, however that it is impossible to estimate the time to collision with a small object. We will see next that binocular information can provide a basis for estimating time to collision with objects of any size.

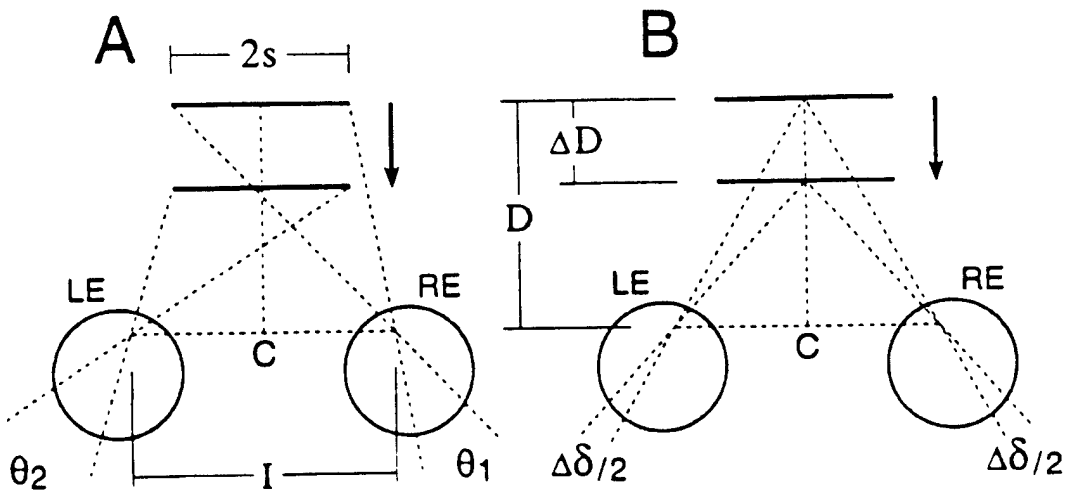

Figure 13 A: An object of width 2s moves at an instantaneous velocity V_Z on a straight line through a point C midway between the eyes. The angular subtense of the object (θ) increases from $\theta 1$ at time $t=0$ to $\theta 2$ at time $t=\Delta t$. B: A point object, located at P at a distance D from the eyes, moves at an instantaneous velocity V_Z on a straight line through a point C midway between the eyes. At time $t=\Delta t$, the object is located at P' and has traveled a distance ΔD. The disparity of the object (δ) relative to a stationary reference mark (M) changes from $\alpha_R + \alpha_L$ at time $t=0$ to $\alpha'_R + \alpha'_L$ at time $t=\Delta t$. The change in disparity ($\Delta\delta$) is equivalent to $\phi' - \phi$. LE: left eye. RE: right eye. I: interpupillary distance.

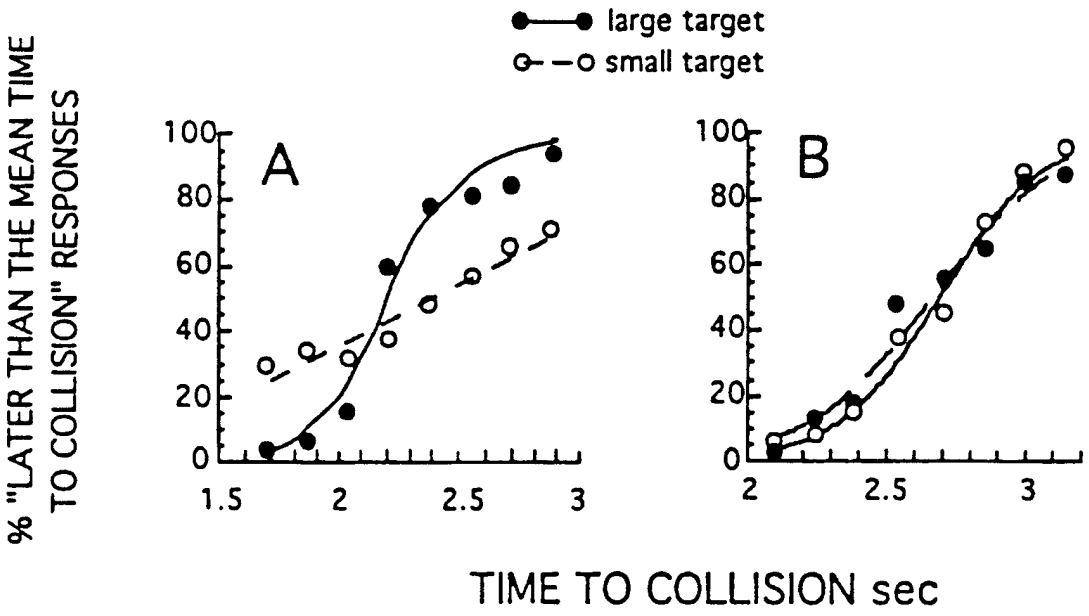

Figure 14 A: Discrimination of trial-to-trial variations in time to collision in case that estimates were based on monocular information only (A) and binocular information only (B). Filled circles are for the large target and open circles for the small target.

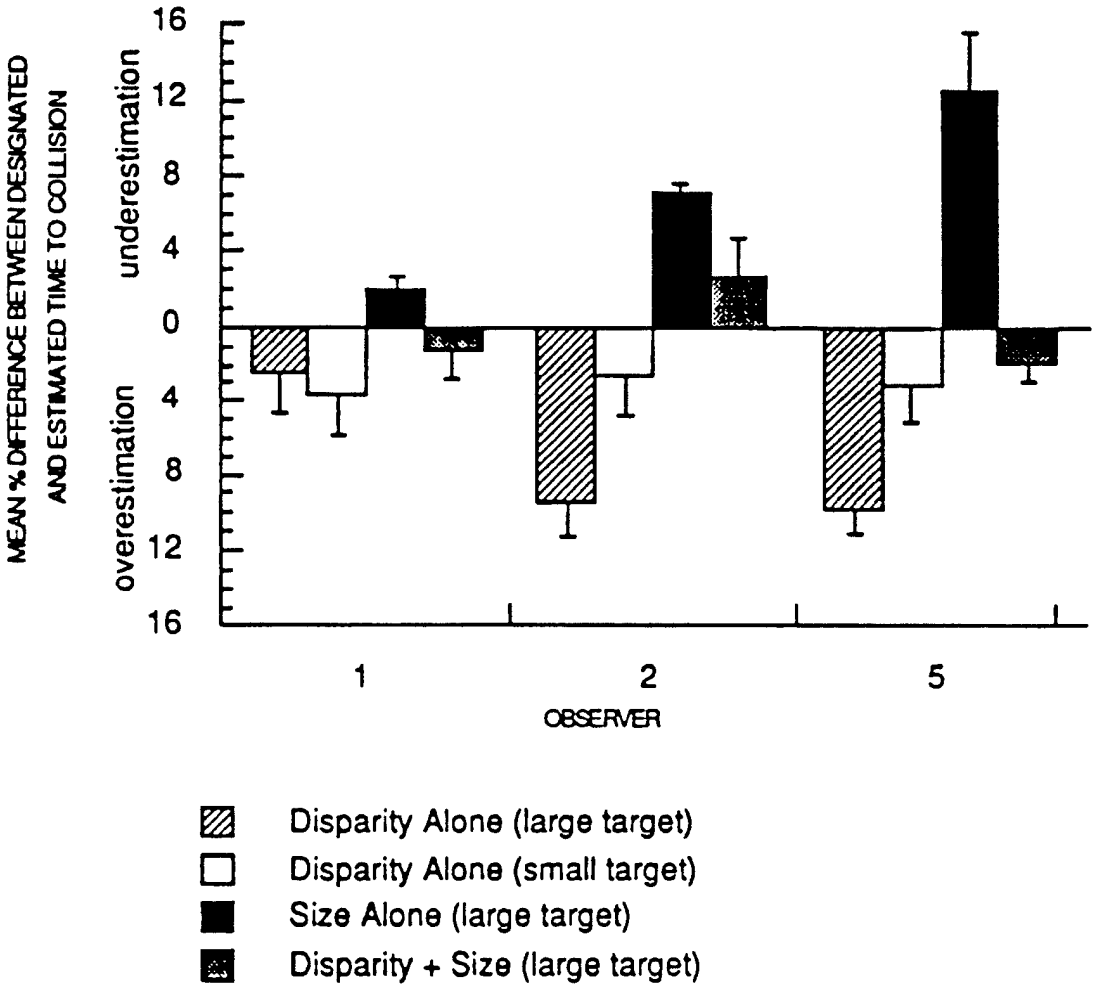

Figure 15. The mean percentage difference (and standard errors) between designated and estimated time to collision for observers 1, 2 and 5. Hatched bars: estimates based on binocular information alone (large target). Open bars: estimates based on monocular information alone (small target). Solid bars: estimates based on monocular information alone (large target). Grey bars: estimates based on combined binocular and monocular information (large target).

It has been shown theoretically that a binocular correlate of time to collision (T) is available for small as well as for large objects (Regan, 1995). In particular

$$T \approx \frac{I}{D(d\delta/dt)} \qquad (3)$$

where D is the object's distance, I is the interpupillary separation and ($d\delta/dt$) is the rate of change of relative disparity (see Fig. 13B). However, although a substantial number of studies on stereomotion have been published [reviewed in Tyler (1991), Regan (1991b) & Collewijn & Erkelens, 1990)], as have a substantial number of studies on time to collision [reviewed in Tresilian (1995)], there have been very few reports of data on the use of binocular information in estimating time to collision. This might seem a curious omission given that the monocularly-available ratio $\theta/(d\theta/dt)$ is an ineffective indicator of time to collision for small objects (Regan & Beverley, 1979). Among the possible reasons for this omission are the following. (a) Viewing distance enters into equation (3), and the weight of evidence is that we are poor at judging the absolute distance of objects further than a few meters away from the head (Collewijn & Erkelens, 1990). (b) The sensation of motion in depth generated by a given rate of change of disparity is quite different in different visual spatial environments. In particular, the sensation of motion in depth is enhanced by the presence of stationary reference marks close to the moving object's retinal images (Tyler, 1975; Erkelens & Collewijn, 1985a, b; Regan, Erkelens & Collewijn, 1986a). (c) Many subjects have areas of the visual field that are selectively blind to stereomotion (Richards & Regan, 1973; Regan, Erkelens & Collewijn, 1986b; Hong & Regan, 1989).

We created retinal images in an observer's left and right eye whose binocular disparity changed in exactly the same way as the retinal images of a spherical object moving directly towards the head at constant speed. Target size

was constant. The stimulus set consisted of 64 different combinations of time to collision [i.e. the ratio I/D(dδ/dt)], disparity displacement (i.e. Δδ, the total change of disparity during a presentation), and presentation duration. Time to collision and disparity displacement varied orthogonally within the stimulus set. We chose to dissociate dδ/dt and Δδ because it has been claimed that discriminations of dδ/dt are based on Δδ rather than on dδ/dt (Harris & Watamaniuk, 1995) — though subsequent studies have shown this claim to lack general validity[6,7]. The observer's task was to signal whether time to collision was shorter than the mean of the stimulus set. Fig. 14(B) shows that discriminations threshold for time to collision was the same for a large (0.7 deg) and small (0.03 deg) target — quite different from the situation when discrimination was based entirely on monocular information [Fig. 14 (A)]

When the same response data were plotted versus trial-to-trial variations in disparity displacement (Δδ) the resulting psychometric function was flat, indicating that the observer ignored Δδ. Stepwise regression analysis confirmed that discriminations were based entirely on time to collision, and that Δδ and presentation duration were ignored.

Although a low discrimination threshold is required for precise estimates of absolute time to collision, a low discrimination threshold does not necessarily imply accurate estimates: estimates might be consistently too long or too short.

We measured the absolute accuracy with which time to collision is estimated when only binocular information is available using a method similar to that already described for the monocular information case. Hatched and open bars in Fig. 15 show errors for the large and small targets respectively.

From the data shown in Fig. 15 plus the results of stepwise regression analysis we concluded that, on the basis of the ratio $I/D(d\delta/dt)$ alone, observers can make accurate estimates of time to collision with an approaching object, whether the object is small or large, and while ignoring simultaneous variations in disparity displacement ($\Delta\delta$), presentation duration and final disparity (Gray & Regan, 1997). Errors were all overestimations. The finding that the accuracy of judging time to collision can be higher for a small than for a large target might be due to the fact that the rate of change of disparity and the rate of change of size provide conflicting information, and that the conflict would be less for a small target, because the $d\theta/dt$ signal was much weaker.

We further concluded that in everyday situations when both monocular and binocular information are available simultaneously, accurate estimates of absolute time to collision, will be based almost entirely on binocular information when the approaching object is small and no more than a few m away.

We went on to measure the absolute accuracy of estimating time to collision in the situation that both binocular and monocular information was available exactly as in everyday conditions. We used the large (0.7 deg) target. The grey bars to the right of the black bars in Fig. 15 shows that errors ranged

from 1.3% to 2.7%. Subjecting the data to repeated-measures ANOVA and post-hoc Tukey test showed that, for the large target, errors in estimating time to collision were significantly lower when estimates were based on both binocular and monocular information than when they were based on either monocular or binocular information alone (Gray & Regan, 1997).

If we assume that a cricket or table tennis player can use visual information up to about 300 msec before the instant of impact with the bat, a 1.3% error approaches the performance required to account for the 2.0 to 2.5 msec accuracy with which, it has been estimated, top sportsplayers judge the time to impact with an approaching ball (Regan, Beverley & Cynader, 1979; Bootsma & van Wieringen, 1990).

2.2 (b) Estimates of time to collision with a rotating nonspherical object.

Long–Term Aims 1.1.1 ©, 1.1.2 (a,b,c); Specific Aims 1.2.6–1.2.8. The project is completed and a paper will be published. Gray, R. & Regan, D. Estimating time to collision with a rotating nonspherical object. Vision Research, in press.

Although the retinal image of a *rotating* nonspherical object that is approaching the eye may change shape when expanding, the retinal image does carry information as to the approximate TTC, especially when the object is not too close. This point can be understood as follows. Consider the flat irregularly–shaped object depicted in Fig. 16 whose relative dimensions in the x, y and z (at right angles to the plane of the paper) directions are 1:1:0.1. Suppose that it remains at a constant distance from the observing eye while rotating about an axis RR′ through its center of mass. Within the meridian

perpendicular to RR′ and at right angles to the paper the angular subtense of the retinal image varies by approximately 10:1 during each rotation: between edge–on (as shown) and side-on. But, provided that the viewing distance is not very short, the change of angular subtense within the meridian parallel to RR′ varies much less. In particular the change of angular subtense during one rotation (i.e. between extreme value of θ_1 and θ_2) is only about 1.1:1 at the distance illustrated, and becomes negligible at long distances.

If the object were approaching the eye at constant speed while rotating, and if the observer could identify the axis of rotation, it would, in principle, be possible to obtain a good approximation to the TTC by attending only to the TTC signaled by the relative rate of expansion within the meridian parallel to the axis of rotation.

Although psychophysical data on the human ability to judge the time to collision with an approaching rigid object that is nonspherical and also rotating are lacking, the results of several previous studies that bear indirectly on the question suggest, that observers would not be able to perform the task.

It is well known that isotropic (i.e. constant–shape) expansion of a retinal image or arbitrary shape commonly produces an impression of motion in depth (Wheatstone, 1852; Johansson, 1964; Regan & Beverley, 1978a,b). However as Poincaré (1913) pointed out, when an object's retinal image is expanding isotropically two quite different explanations are geometrically possible: the object might be physically changing size; or the object might be moving in depth. (And, of course, combination of the two cannot be

distinguished using only the information contained in a single two–dimensional retinal image). Poincaré suggested that the brain resolves the ambiguity between changes in an object's size and changes in its distance by utilizing visual changes produced by active exploratory head movements. A different explanation for the same problem, put forward by Fiandt and Gibson (1959) was that, "the perspectives of rigid objects constitute one kind of stimulus for vision and that the other group, the 'rubbery transformations', constitute another kind of stimulus for vision". According to Johansson (1964), both of these hypothesis have the weakness that they do not adequately deal with the perception of combined motion and form changes.

Beverley and Regan (1979a) proposed a quite different explanation. Pointing out that an object moving towards the observer not uncommonly calls for a rapid motor response such as evasion, they suggested that in evolutionary terms there might be some competitive advantage to the organism whose visual system was biased to produce a "safest guess" percept in response to isotropic expansion of an object's retinal image. By not submitting an isotropically–expanding retinal image to leisurely cognitive evaluation, such as a bias would ensure an unthinkingly and unhesitatingly rapid response to a predator approaching on a collision course. The occasional aberrant response to an expanding object would be a small price to pay for the certainty of rapid defensive reaction to real threat. In support of their suggestion they reported that the effectiveness of retinal image expansion as a stimulus for motion in depth perception was severely reduced when the shape of the objects

retinal image changed during expansion (Retinal image dynamics of this kind does not correspond to an approaching predator on a collision course).

In a later investigation of this effect, Beverley and Regan (1980) reported a strong across-meridians nonlinear interaction. In particular, visual responses to expansion of the horizontal angular diameter (θ_H) of the retinal image were considerably affected by the value of $\theta_V/(d\theta_V/dt)$, and responses to expansion of the vertical angular diameter (θ_V) were considerably affected by the value of $\theta_H/(d\theta_H/dt)$. In particular, there was a considerable change in the response to retinal image expansion when $\theta_V/(d\theta_V/dt)$ was equal to $\theta_H/(d\theta_H/dt)$. The significance of this finding is that $\theta_V/(d\theta_V/dt)$ is the TTC for the vertical diameter of the retinal image and $\theta_H/(d\theta_H/dt)$ is the TTC for the horizontal diameter of the retinal image. Beverley and Regan concluded that the TTCs for the horizontal and vertical meridians must have been computed before the stage at which the motion-in-depth signal was generated.

Thus, if it is the case that observers estimate TTC on the basis of the perceived speed of motion in depth, then observers will not in general be able to estimate accurately the TTC with a rotating nonspherical object because motion-in-depth perception is severely affected when a shape change accompanies expansion (Regan & Beverley, 1978a, Beverley & Regan, 1979a) — even though the relative rate of dilation within the meridian parallel to the axis of rotation does signal the approximate TTC.

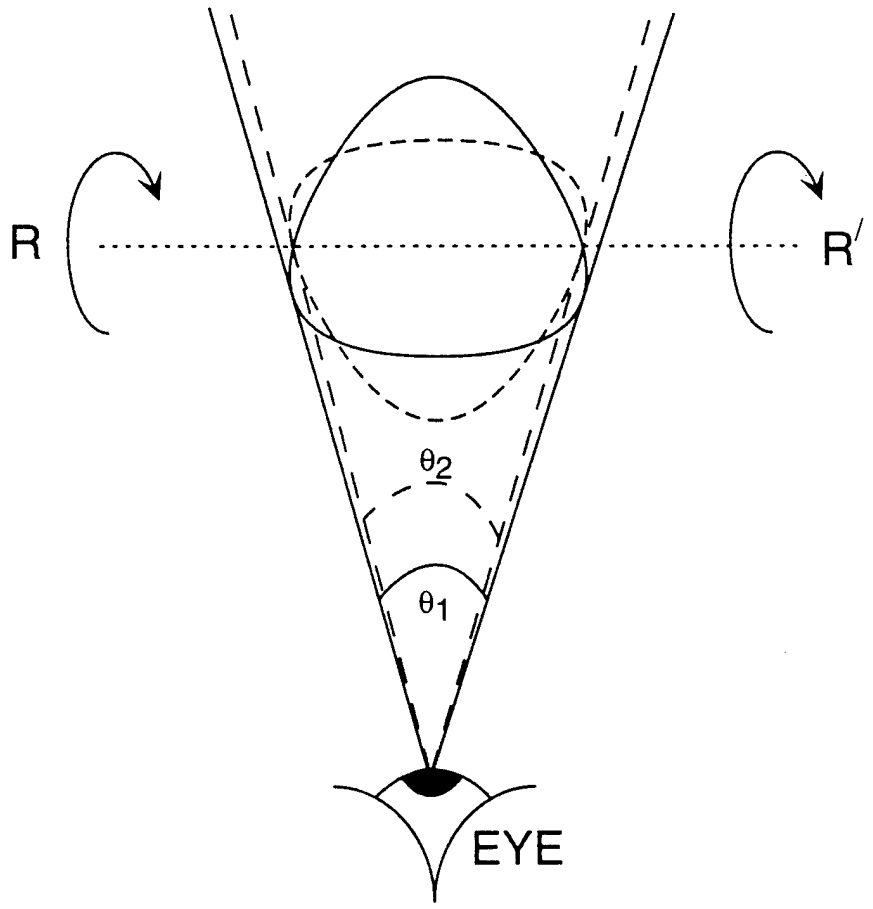

Figure 16. A rotating irregularly–shaped object.

We used the following two kinds of simulated approaching object: a rigid spherical object and a rotating nonspherical object. For simplicity we chose, as the simulated approaching nonspherical object, a tumbling rigid oblate spheroid (i.e. a three-dimensional shape like a blunt-ended version of a rugby ball or American football).

We simulated a rotating approaching oblate spheroidal object that slowly (0.2 rotations/sec) rotated through 90 deg during the maximum value of presentation duration (1.25 sec). The two rotation cases were: (1) a spheroid

initially viewed end-on that rotated 90 deg about its horizontal axis so that it was eventually viewed side–on (Fig. 2, "END–SIDE"); (2) a spheroid initially viewed side-on that rotated 90 deg about its horizontal axis so that it was eventually seen end-on (Fig. 2, "SIDE–END"). In the "END–SIDE" condition the vertical meridian expanded more quickly than the horizontal meridian, while in the "SIDE–END" condition the vertical meridian expanded more slowly than the horizontal meridian. The simulated approaching sphere is illustrated in Fig.2: "SPHERE". Figure 17 brings out the point that the shorter diameters (the horizontal diameters) were the same for the three targets both at the start of the presentation (top row) and also after 1.25 sec (bottom row) and, therefore, provided identical information about TTC in all three simulation conditions. For completeness, we also measured responses to a simulated rapidly–rotating (10 times faster, i.e. two rotations per sec) approaching nonspherical object that completed one or more complete rotations during its approach.

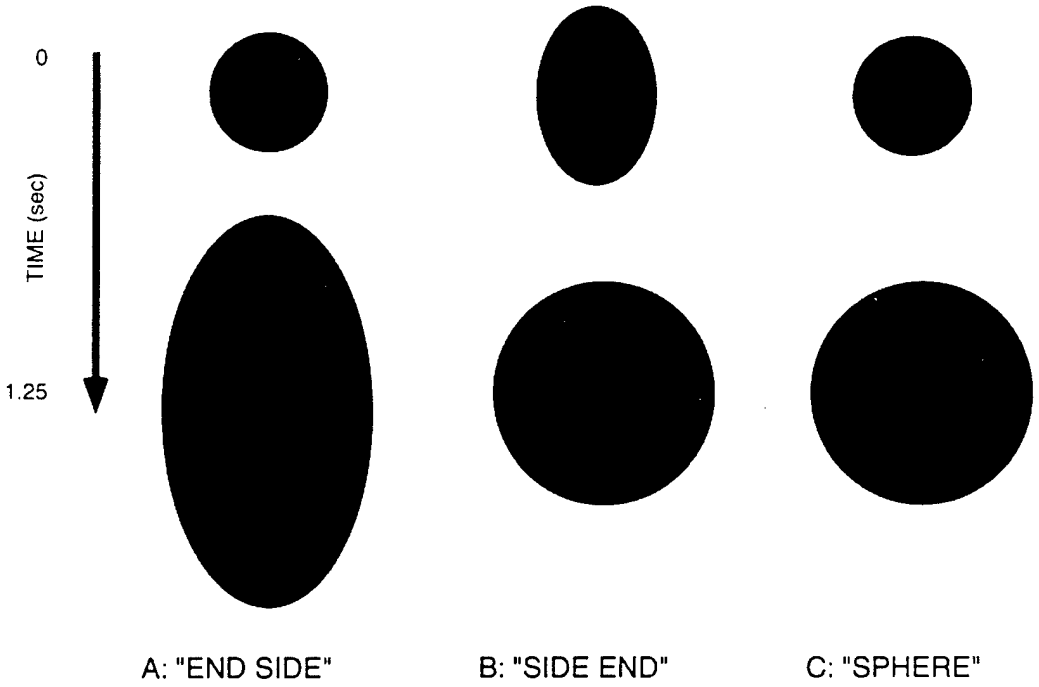

Figure 17. Simulations of an approaching tumbling oblate spheroid and an approaching sphere.

Our aim was to measure the error in estimating absolute TTC for the three kinds of retinal image expansion illustrated in Fig. 2 in the following conditions: both binocular and monocular information were available; only monocular information was available. We also measured errors in estimating absolute TTC for a simulated approaching sphere with binocular information as the only cue to TTC.

We used a multiple–staircase tracking procedure to measure estimated time to collision. The procedure is described fully in Gray & Regan (1998). In brief, the target was presented for a duration that varied from 0.5 to 0.9 sec. Some time after the target had disappeared (at the designated time to collision)

the computer that controlled the experiment triggered a brief click whose timing could be set to within 0.001sec. The observer's task was to press one of two buttons according to whether he judged that the simulated object would have arrived before or after the click. Nine staircases were interleaved in any given run. We used three values of $(\theta_H)_{t=0}$ (0.40, 0.65 and 0.90 deg), and three fixed values of designated time to collision (1.8, 2.2 and 2.6 sec.). No feedback was provided.

Table 1

Observer	Condition	Most Sig. Variable	R^2	Next Most Sig. Variable	R^2
1	Monocular "END-SIDE"	$\theta_H/(d\theta_H/dt)$	0.75	NA	NA
	Monocular "SIDE-END"	$\theta_H/(d\theta_H/dt)$	0.42	$d\theta_H/dt$	0.80
	Monocular "SPHERE"	$\theta_H/(d\theta_H/dt)$	0.91	NA	NA
	Monocular [Fast Rotation]	$\theta_H/(d\theta_H/dt)$	0.86	$\Delta\theta$	0.91
1	M & B "END-SIDE"	$\theta_H/(d\theta_H/dt)$	0.86	NA	NA
	M & B "SIDE-END"	$\theta_H/(d\theta_H/dt)$	0.79	NA	NA
	M & B "SPHERE"	$\theta_H/(d\theta_H/dt)$	0.89	Δt	0.93
	M & B [Fast Rotation]	$\theta_H/(d\theta_H/dt)$	0.81	NA	NA
	Binocular [Constant shape and size]	$I/[D(d\delta/dt)]$	0.83	NA	NA
2	Monocular "END-SIDE"	$\theta_H/(d\theta_H/dt)$	0.73	NA	NA
	Monocular "SIDE-END"	$\Delta\theta_H$	0.55	TTC	0.84
	Monocular "SPHERE"	$\theta_H/(d\theta_H/dt)$	0.87	NA	NA
	Monocular [Fast Rotation]	$\theta_H/(d\theta_H/dt)$	0.8	NA	NA
2	M & B "END-SIDE"	$\theta_H/(d\theta_H/dt)$	0.78	$\Delta\theta$	0.90
	M & B "SIDE-END"	$\theta_H/(d\theta_H/dt)$	0.75	Δt	0.87
	M & B"SPHERE"	$\theta_H/(d\theta_H/dt)$	0.80	NA	NA
	M & B [Fast Rotation]	$\theta_H/(d\theta_H/dt)$	0.73	$\Delta\theta$	0.79
	Binocular [Constant shape and size]	$I/[D(d\delta/dt)]$	0.85	NA	NA

Columns 3-6 in Table 1 set out the results of subjecting the response data to stepwise regression analysis. The main psychophysical finding was that observers could not perform the task at all or, at best, performed poorly in the "SIDE–END" condition of nonisotropic expansion when estimates of TTC were based on monocular information only. For observer 1, the task-relevant variable accounted for only 42% of the variance, while the task–irrelevent variable $d\theta_H/dt$ accounted for a considerable amount of additional variance. For observer 2, a task–irrelevent variable ($\Delta\theta_H$) accounted for most of the variance. Performance was good in all other conditions, the task-relevant variable accounting for a high proportion of the total variance.

Fig.18(A) shows errors in estimating time to collision for observer 1 in the condition that estimates were based on monocular information only. In accord with most (Schiff & Detwiler, 1979; Cavallo & Laurent, 1988; Gray & Regan, 1998), but not all (Heuer, 1993) previous reports, the TTC with the simulated approaching spherical object was underestimated. For observer 1, the underestimation was 8.5%.

Allowing for the fact that the TTC for the "SPHERE" stimulus itself was underestimated, the total error for the "END–SIDE" stimulus was a 17% underestimation. For the "SIDE–END" stimulus, stepwise regression analysis showed the TTC estimates to be unreliable (see below), because the observer

was strongly influenced by task–irrelevent variables: these data are marked NR (not reliable) in Fig.18(A).

Fig.18(C) shows that observer 2 gave similar results. The perceived TTC for the "END–SIDE" stimulus was a 13.6% underestimate of the correct value, an error that was significantly greater (by 7.4%) than the perceived TTC for the isotropically–expanding "SPHERE" stimulus.

In the "monocular information only" condition, the rapidly–rotating nonspherical simulated object had essentially the same perceived time to collision as the simulating spherical object [observer 1: $t(52)=1.1$, $p>0.2$; observer 2: $t(52)=0.69$,$p>0.2$].

Fig.18(B) & (D) shows errors in estimating time to collision in the conditions that either binocular information alone or both binocular and monocular information were available. Fig.18(B) & (D) shows that the addition of binocular to monocular information dramatically improved the accuracy of estimating absolute time to collision not only (as reported previously) for the simulated spherical object (Gray & Regan, 1998), but also for the simulated rotating nonspherical object. More importantly, in the "SIDE–END" simulation condition the addition of binocular to monocular information enabled the observers to perform the task correctly by ignoring task–irrelevent variables.

We used a repeated–measure ANOVA to compare, over all condition used, errors in estimating TTC, entering INFORMATION (monocular versus monocular plus binocular) and CONDITION ['SPHERE", "END–SIDE"; "SIDE–END"; "RROT", i.e. fast rotation]. When both binocular and monocular information was available, errors were significantly smaller than when only

monocular information was available [$F(1,1)=67$, $p<0.05$]. Errors were also significantly smaller in the isotropic–expansion ("SPHERE") condition than in the conditions of non-isotropic expansion [$F(3,3) = 10.38$, $p<0.05$].

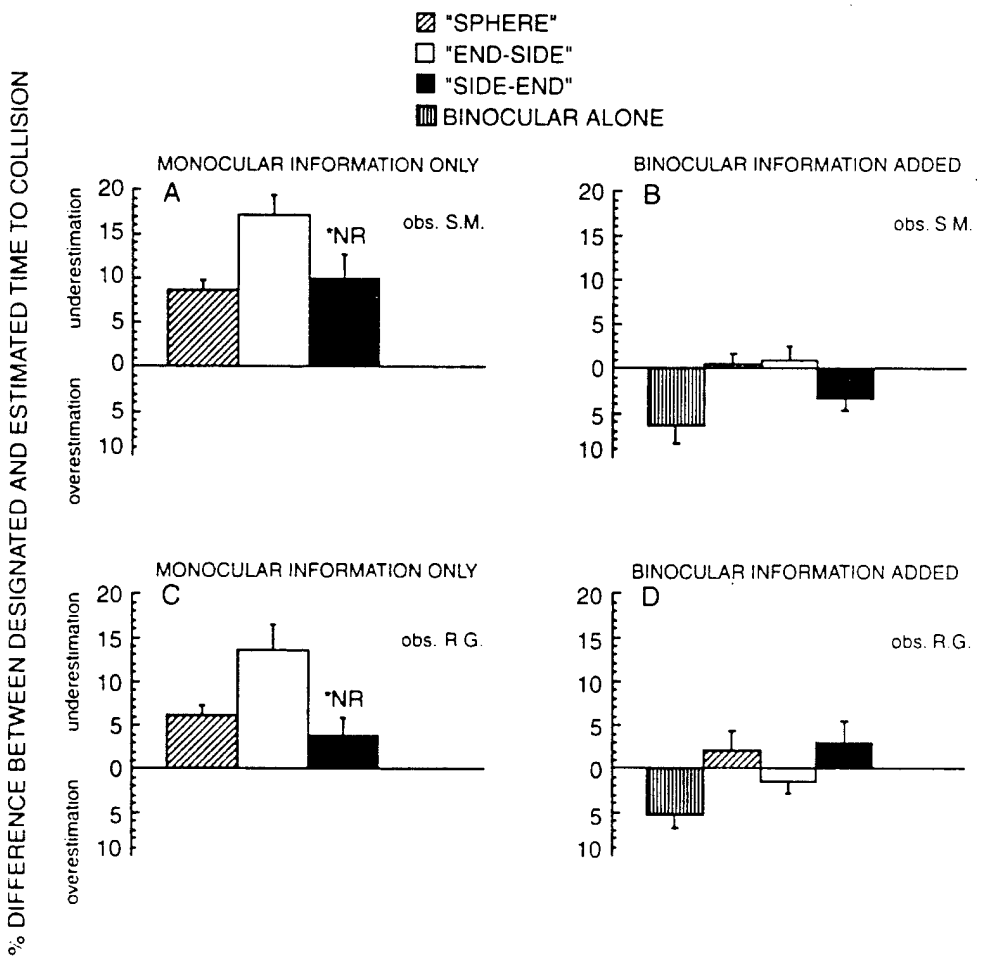

Figure 18. Errors in estimating time to collision for a simulated spherical approaching object "SPHERE' and for a simulating approaching nonspherical object that was rotating slowly "END–SIDE" and "SIDE–END". A,C: only monocular information available. B,D: binocular and monocular information available. In the "binocular alone" condition, the simulated object was spherical and did not expand. *NR signifies that the measurement was not reliable: one observer placed more weight on a task–irrelevent variable than on the task–relevent variable; the other did not ignore task–irrelevent information. A,B: observer 1. C,D: observer 2.

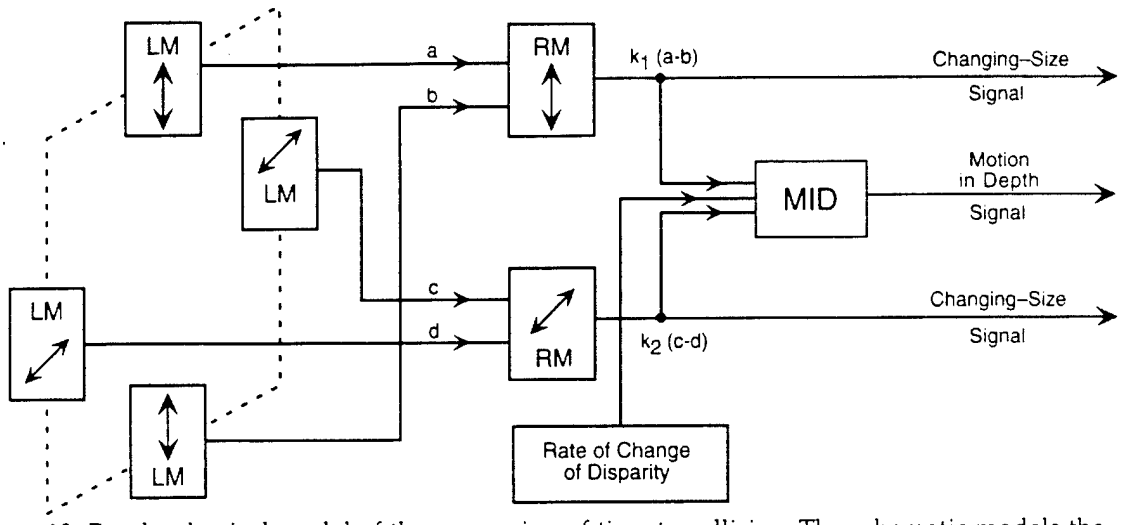

Figure 19. Psychophysical model of the processing of time to collision. The schematic models the boundaries of a solid untextured rectangular retinal image are shown by the dashed line. LM: Filters that respond to local motion along the arrowed line. Their outputs (*a*, *b*, *c*, *d*) assume a magnitude that is linearly proportional to local speed and a sign that corresponds to the direction of motion. RM: One–dimensional filters whose outputs signal the speed and sign (i.e. expansion vs. contraction) of relative motion along some given retinal meridian. MID: Two–dimensional relative motion filter that is most efficiently excited by expansion of the retinal image when the expansion is not accompanied by shape change [i.e. provided that $k_1(a - b) = k_2 (c - d)$, where k_1 is inversely proportional to the height of the image and k_2 is inversely proportional to its width]; the output of the MID stage signals motion in depth. The MID filters also receives input from a filter whose output signals the rate of change of relative disparity.

We conclude that, although observers can estimate absolute time to collision with good accuracy using monocular information alone when the approaching object is spherical, they may be unable to reliably and accurately estimate absolute time to collision when a nonspherical object makes only part of a rotation during the viewing time in the condition that only monocular information is available.

Even when estimates of TTC are based chiefly on monocular task–relevent information rather than monocular task–irrelevent variables [as for the "END–SIDE" type of expansion illustrated in Fig. 16], estimates may be

wrong by up to 17%. The situation is qualitatively worse for the "SIDE–END" kind of retinal image expansion depicted in Fig.16: observers are unable to ignore task–irrelevent variables and may even base estimates on a task–irrelevent variable. This failure is consistent with the previous proposal that the motion–in–depth cue to TTC is severely degraded when the fractional rate of expansion of an object's retinal image is considerably smaller along one meridian than along a perpendicular meridian (Beverley & Regan, 1979a).

By utilizing binocular information the capability of making reliable and accurate estimates of TTC can be restored in the case of the "SIDE–END" target, and errors in estimating time to collision can be reduced considerably in the case of the "END–SIDE" target.

We should note, however, that although visual sensitivity to changing-disparity can extend well beyond the roughly 10m range of stereoacuity (Regan, Kaufman & Lincoln, 1986), this extension of range is governed by a tradeoff between the object's speed and the square of its distance, so that useable binocular information is still restricted by the distance of the approaching object. Therefore, in practice it may be necessary for the observer to monitor information about time to collision on a moment-by-moment basis, because the binocular information required to correct the misleading monocular information may not be available until very shortly before completing the motor action required to avoid or achieve collision.

On the face of it, our proposed explanation for errors in estimating absolute TTC in the "SIDE–END", and "END–SIDE" conditions of a slowly–rotating nonspherical approaching object on the basis of monocular

information is not consistent with our finding that errors were small when the simulated rapidly–rotating nonspherical target completed one or more rotations during its approach. The relative rate of expansion within the vertical and horizontal meridians would differ throughout the approach, just as it does in the "SIDE–END" and "END–SIDE" conditions. To account for our finding with the simulated rapidly–rotating nonspherical object, we suggest that the integration time constant of the nonlinear interaction between the relative rates of expansion demonstrated previously (Beverley & Regan 1979a, 1980) is of the order of the 0.5 sec rotation period of our simulated rapidly–rotating object. This provides experimental support for Tresilian's (1991) speculation that when processing TTC, the visual system averages over rotations.

In a series of papers we have developed a model, schematically outlined in Fig.19, of the early visual processing of the changing–size and changing–disparity information in the retinal images of an approaching untextured object, and the consequent generation of motion-in-depth perception (Beverley & Regan, 1979a,b, 1980, 1983; Regan & Beverley, 1978a,b, 1979a,b, 1980, 1981; Regan et al., 1986; Regan & Hamstra, 1993; Regan & Vincent, 1995; Vincent & Regan, 1997). In this paper we report that the binocular (RATE OF CHANGE OF DISPARITY) input in Fig.19 to the stage at which the motion in depth signal in generated (MID) assumes an important role when the approaching object is nonspherical and rotating especially when the rate of rotation is low.

Errors in estimating absolute time to collision in the "monocular information only" condition fell short of what one would expect if perceived

time to collision were based on the mean of the different times to collision signaled by the rates of expansion of the diameter of the retinal image in different meridians. For example, in the "END–SIDE" condition depicted in Fig.17, θ_V increased by a factor of 3.4 while θ_H doubled, whereas in the "SPHERE" condition both θ_V and θ_H doubled. If perceived TTC were based on the average of θ_H /($d\theta_H$ /dt) and θ_V /($d\theta_V$ /dt), then we would expect that perceived TTC for the "END–SIDE" target would be roughly 33% less than for the "SPHERE" target. But the difference was only about 8% of the designated TTC. To account for this finding we assume that, when only monocular information is available, the perceived TTC is determined by an average of $\theta/(d\theta/dt)$ over different meridia of the retinal image (where θ is the instantaneous angular diameter of the retinal image along a given meridian) and that the averaging process assigns different weights to different values of $\theta/(d\theta/dt)$. This suggestion is consistent with previous evidence (Beverley & Regan, 1979a; Beverley & Regan, 1980).

Fig. 18(A) - (D) shows that, in the case of isotropic expansion ("SPHERE"), TTC is underestimated when only monocular information is available and overestimated when only binocular information is available, and that when both monocular and binocular information is available the total error is roughly equal to the algebraic sum of the two component errors. This is not the case when binocular and monocular information are combined for the "END–SIDE" kind of nonisotropic expansion illustrated in Fig. 17; a comparison of the white bar in Fig. 18(A) with the hatched and white bars in

Fig. 6(B) indicates that the binocular information dominates. The same conclusion held for observer 2 [Fig. 18(C) & (D)]. We conclude that the two kinds of information are weighted roughly equally when expansion is isotropic, but when expansion is nonisotropic, as in Fig. 16(A) & (B), binocular information is weighted more heavily than monocular information. This unequal weighting has the effect of favouring the more unequivocal and hence more reliable information.

Summary

We conclude that when attempting, on the basis of monocular information (tau) alone, to estimate the time to collision with an approaching nonspherical object that is rotating slowly, observers are either unable to perform the task at all, or make large errors. When stereo information is added, estimates become accurate. Implications include the following. (1) Players attempting to catch a tumbling American football or a tumbling Rugby ball are commonly advised to keep their eyes on the ball right up to the last instant of its flight. We assume that the reason for this common wisdom is that stereo information is only available at close range. (2) Highway drivers who lack stereoscopic depth perception might be at a disadvantage when attempting to merge safely with traffic on a rotary. (3). Simulators for training medical emergency helicopter pilots to thread through high-rise buildings en route to landing on the roof of a downtown hospital might be more effective if they provide stereo as well as monocular information.

Theoretical Discussion

Many textbooks have been written on the analysis of human-designed linear systems and the various methods are highly developed and well understood (e.g., Aseltine, 1958; Bracewell, 1965; White & Tauber, 1969). The charm of linear systems analysis is that one method applies to any system provided that the system is linear. Nonlinear systems analysis is a different proposition: there are an indefinitely large number of kinds of nonlinear systems; no method is valid for all the different kinds; and the mathematical challenges can be far more severe than in linear systems analysis. But both the static and dynamic behaviour of a linear system is severely restricted, and its range of possible behaviours is narrow (Hirsch & Smale, 1974). And, as noted by Reichardt and Poggio (1981, p. 187), writing on the topic of neural information processing, " - - every nontrivial computation has to be essentially nonlinear, that is not representable (even approximately) by linear operation".

One general approach to the understanding of complex human-designed nonlinear systems is called structural analysis. A second general approach is called functional analysis or mathematical analysis. In the analysis of a multi-input multi-output system the aim of this second kind of nonlinear systems analysis is to write equations that allow the system's outputs to be predicted from a knowledge of the system's inputs. The resulting functional model may contain many subsystems, even parallel sequences of subsystems, to each of which is assigned an equation relating its output to its input. (Blaquière, 1966; White & Tauber, 1969). In complex nonlinear human-designed systems it is in general a nontrivial task to relate structure to function or to relate

function to structure. For example a nonlinear system may have properties that cannot, in principle, be assigned a location within the system. And the sequence of processing in the functional model may have little relation to the physical layout of the system's component parts.

Turning to the analysis of complex nonlinear biological systems, the structural and functional approaches are, perhaps, best regarded as complementary (Mountcastle, 1979; Marmarelis & Marmarelis, 1978). In vision research, the psychophysical approach corresponds to functional nonlinear systems analysis. Fig. 19 sets out our proposed functional model of the physiological system that underlies our perception of motion in depth and estimates of time to collision with an approaching object. As with any other functional model it is a theoretical construct, and there is no general requirement to bear in mind the physical structure of the system when designing the model. Our model contains several subsystems, some of whose behaviour is approximately linear and one of which is strongly nonlinear. The following is a brief outline.

The boxes marked LM respond to local motion along a particular direction, and signal both direction (e.g., leftwards, rightwards) and speeds. Either Reichardt or Elaborated Reichardt detectors would fill the requirement for the LM subsystems (Reichardt, 1961, 1986; Van Santen & Sperling, 1985). There is evidence that for input speeds appreciably greater than zero the output of an LM box is linearly related to its input to within ± 5%, and that an essential nonlinearity that is evident when retinal image speed is close to zero is

linearized by the instability of the retinal image that is present when the head is not on a bite bar (Regan & Beverley, 1980).

An RM subsystem rejects any common component of velocity signaled by the two LM subsystems that feed it; its output is proportional to the difference between the velocities of retinal image contours at two locations (Beverley & Regan, 1979b; Regan & Beverley, 1978a, 1980). The output of an RM subsystem is scaled by a factor k that is inversely proportional to the distance between the two LM subsystems that feed it. Thus, the output $[k_1(a-b)]$ of the upper RM box in Fig. 7 is proportional to tau for the vertical meridian of the dotted image, and the output $[k_2(c-d)[$ of the lower RM box is similarly proportional to tau for the horizontal meridian of the dotted image (Regan & Hamstra, 1993).

The MID subsystem is Fig. 19 generates an output that supports the perception of motion in depth (Regan & Beverley, 1979b). But retinal image expansion does not necessarily generate an output from the MID box. The two-dimensional organization of image expansion is a major factor. The MID subsystem contains a nonlinear element that distinguishes between isotropic and nonisotropic expansion of an object's retinal image (Beverley & Regan, 1979a, 1980). The input to this nonlinear element is some relation between $k_1(a-b)$ and $k_2(c-d)$ such as their ratio or their difference. Optimal response to retinal image expansion is obtained when their ratio is unity, i.e. their difference is zero. A comparison of our findings for slow rotation and fast rotation offers some insight into the dynamics of this nonlinearity. In the SIDE-END and END-SIDE conditions (Fig. 17) we supplied a transient (i.e.

nonrepetitive) input to the nonlinear element. The result was that the MID stage did not respond to retinal image expansion in the same way as when expansion was isotropic: observers reported that the resulting perception of motion in depth was weak. In the 2.0 Hz rapid–rotation condition (RROT) the ratio (and the difference) between k_1(a-b) and k_2(c-d) oscillated at 2.0 Hz. The MID subsystem was not disabled, and a transient ramp of retinal image expansion produced an output from the MID subsystem. We conclude that the nonlinear element within the MID subsystem was unable to respond to this 2Hz variation and, therefore, has a time constant of more than 0.5 sec. Next we note that the generation of a motion–in–depth signal by the MID subsystem fails at approximately 2Hz when the eye is stimulated by isotropic oscillations of size, so that this process also has a time constant of roughly 0.5 sec (Regan & Beverley, 1979b, Fig. 3). As a result of this sluggish time constant, the output of the MID subsystem produced by the transient ramp of expansion in the RROT condition is, in effect, time-averaged to give an accurate representation of tau.

2.2 (c) Simulation of motion in depth: Importance of accurately matching texture dynamics to rate of expansion of the approaching object's retinal image

Long-Term Aim 1.1.1 (c); Specific Aim 1.2.6

Two papers have been published: Vincent, A. & Regan, D. (1997). Judging the time to collision with a simulated textured object: effect of mismatching rates of expansion of size and of texture elements. Perception and Psychophysics *59,32-36., Gray, R. & Regan, D. (1998). Motion in depth: adequate and inadequate simulation.* Perception and Psychophysics, *61, 236-245.*

Relevance: Because of current limitations of both display technology and computer graphics algorithms, the visual displays in flight simulators fall short of realistic depictions of the out-of-cockpit scenes viewed by pilots of real aircraft. A pilot must use time to collision information very accurately and precisely to avoid collision with terrain features and also to avoid rear-end collisions with another aircraft when maneuvering. However, in designing flight displays, compromises have been made in simulating what a pilot sees when closing on a textured object, and these compromises have so far been made without adequate knowledge of visual function. The relevance of the following studies is to better inform these compromises.

We previously developed hardware of our own design that displayed a textured expanding target for which the rate of expansion of texture elements could be dissociated from the target's rate of expansion, and showed that, when the rate of expansion of texture elements was less than the target's rate of expansion, the human motion-in-depth system was only weakly stimulated [Beverley & Regan (1983) Texture changes versus size changes as stimuli for motion in depth. Vision Research, 23, 1387-1400]. Recently we used this stimulator in combination with our tracking technique for measuring errors in estimating absolute time to collision, and found that a mismatch between the rates of expansion of texture element size and object size caused significant errors[4].

In view of the fact that many investigators of heading and of motion-in-depth have used flow fields created from dot patterns where the dots remained constant in size, we investigated the implication of our finding that the results

of such experiments might have restricted application in everyday real-world conditions.

Our original stimulus was an expanding square covered by rectangular black and white texture elements of randomly-determined shape and size. With this stimulus both texture element size and the distance between texture elements are mismatched, but with a constant-size dot display the distance between dots is not mismatched. Accordingly, we developed a textured display in which the rate of expansion of the following could be varied independently: target size; dot size; distance between dots.

We found that significant errors in estimating absolute time to collision are produced when dot size is constant instead of expanding in accord with target size. However this effect only occurs for dots larger than 2.2 - 4.4 min arc. For smaller dots, holding dot size constant does not produce significant error[14].

2.2.(d) Adaptation to retinal image expansion causes errors in estimating time to collision

Long-Term Aims 1.1.1(c), 1.1.2(a); Specific Aim 1.2.6. This project has been completed, and a paper has been published. Gray, R. & Regan, D. (1999). Adapting to expansion increases perceived time to collision, Vision Research, 39, 3602-3607.

Relevance : This is a possible cause of rear-end collisions when overtaking on the highway and in collisions with ground features in NOE flight.

We proposed that the perceived speed of an approaching object's motion in depth is determined, not by the object's actual speed, but rather by its time to collision (Regan & Hamstra, 1993). It is known that adaptation to an expanding

retinal image reduces the perceived speed of subsequently-viewed expanding targets (Regan & Beverley, 1979). Putting together these two points, the possibility arises that prolonged viewing of approaching objects might cause errors in estimating time to collision.

Using the procedure described in Section 4.2 (a) we compared errors in estimating absolute time to collision with a simulated approaching object before and after adaptation to retinal image expansion. Estimated time to collision was longer by 18 to 25% after adaptation.

Our findings suggest that if, after a period of high-speed driving while looking ahead at an empty road, a driver comes up on a more slowly-moving vehicle, the driver might overestimate the time to collision while attempting to overtake and thus be at risk of a high-speed rear-end collision.

2.3 Cyclopean processing of motion

2.3.(a) Cyclopean processing of motion in depth

A referee challenged our findings in References 6 & 7, and required us to discuss our data on speed discrimination for cyclopean motion-in-depth in the light of the conclusion of Harris & Watamaniuk (Vision Research ,1995, 35, 885-896) that there is no binocular mechanism sensitive to the speed of motion-in-depth and that cyclopean discriminations are based on displacement rather than speed. We repeated the Harris & Watamaniuk experiment and confirmed their findings. However, their experiment was restricted to the special case that the cyclopean target passes through zero disparity and, therefore, disappears and reappears midway through its trajectory. Not surprisingly, this

disappearance and reappearance hinders the operation of the motion-in-depth mechanism, possibly by setting the cyclopean system a sudden correspondence problem.

We developed a new experimental design that allowed us to show that there are separate mechanisms for discriminating cyclopean speed and displacement in depth. The stimulus array consisted of 64 combinations of rate of change of disparity, disparity displacement, and presentation duration. After each presentation the observer was instructed to signal (1) whether the speed of motion in depth was faster than the mean for the stimulus set, and (2) whether the distance moved during the presentation was larger than the mean for the stimulus set. Fig. 20 shows that observer could discriminate speed while ignoring distance moved (A & B), and that they could discriminate distance moved while ignoring speed (C & D).

Our evidence shows that the conclusion of Harris and Watamaniuk is in general incorrect. Our evidence shows that there is a cyclopean mechanism sensitive to the speed of motion-in-depth that functions well in the situation that the target remains visible throughout its trajectory-whether motion in approaching or receding, and whether disparity is crossed or uncrossed.

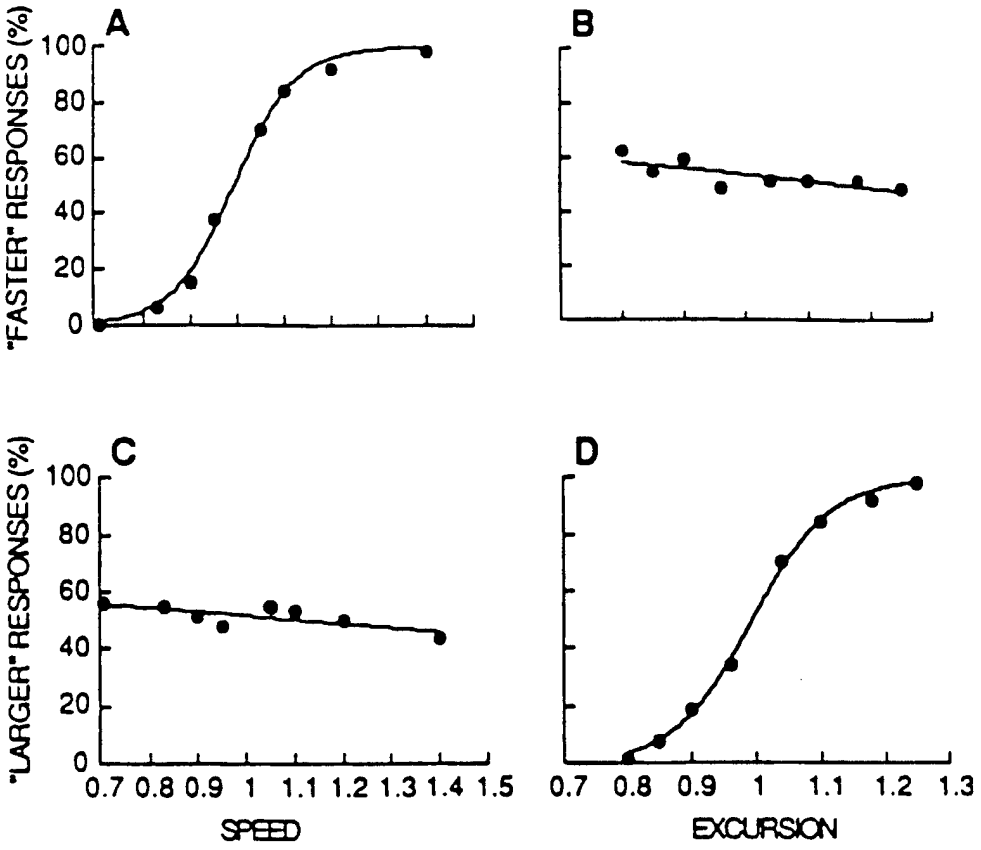

Figure 20. Discrimination of simultaneous trial-to-trial variations of both the rate of change of disparity $d\delta/dt$ (A & B) and the displacement $\Delta\delta$ (i.e. excursion, C & D) of motion in depth for a cyclopean target. The target started at 5 min arc near disparity and moved towards the observer. From Portfors, C. V. and Regan, D. (1997). Just-noticeable difference in the speed of cyclopean motion in depth and the speed of cyclopean motion within a frontoparallel plane. *Journal of Experimental Psychology: Human Perception and Performance*. 23: 1074-1086.

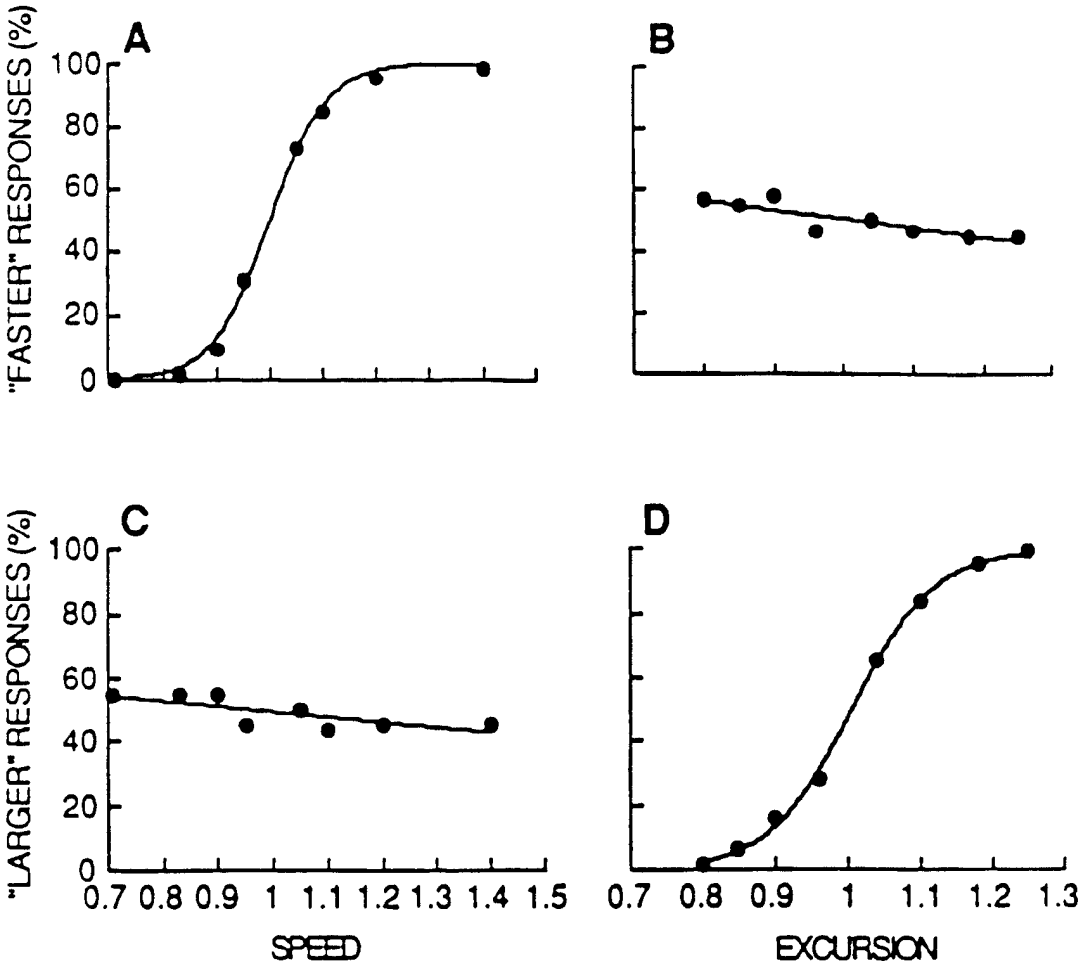

Figure 21. Discrimination of simultaneous trial-to-trial variations of both the speed $d\phi/dt$ (A & B) and the displacement $\Delta\phi$ (i.e. excursion, C & D) of the motion within a frontoparallel plane of cyclopean target. The target was at 10 min arc disparity and moved upwards, away from the fovea. From Portfors, C. V. and Regan, D. (1997). Just-noticeable difference in the speed of cyclopean motion in depth and the speed of cyclopean motion within a frontoparallel plane. Journal of Experimental Psychology: Human Perception and Performance. 23: 1074-1086.

2.3.(b) Cyclopean processing of motion parallel to the frontal plane.

This project is completed and a paper has been published: Kohly, R. & Regan, D. (1999). Evidence for a mechanism sensitive to the speed of cyclopean form. Vision Research, 39, 1011-1024.

In Reference 7 we had developed a method for showing that observers can discriminate the speed of a cyclopean target moving parallel to the frontal plane while ignoring the distance moved, and at the same time discriminate the distance moved while ignoring speed. The method was analogous to that just described, and results are shown in Fig. 21.

A referee challenged our findings in Reference 7, and required us to discuss our data on speed discrimination for cyclopean motion within a frontoparallel plane in the light of the conclusion of a manuscript that had been submitted to *Vision Research* and was sent to us by the referee. The manuscript concluded that for the generality of observers there is no cyclopean mechanism for motion within the frontoparallel plane. It has since been published (Harris & Watamaniuk, *Vision Research* (1996), 36, 2149-2157). Since we had used a sharp-edged cyclopean bar to find evidence that all our 6 observers had a sensitive cyclopean speed mechanism, while Harris & Watamaniuk (1996) had used a cyclopean grating when finding that neither of their two subjects were able to discriminate speed, we were left with no alternative but to suggest that the cyclopean speed mechanism we had demonstrated is only effective for sharp-edged targets, i.e. for form defined by an abrupt change of disparity.[7]

We therefore measured speed discrimination thresholds for motion of a cyclopean grating parallel to the frontal plane using an experimental design that allows us to show that all task-relevant cues are ignored. We found 11 observers who have a sensitive cyclopean speed mechanism for moving gratings, thus indicating that the conclusion of Harris & Watamaniuk (1996) is

not generally correct. A few observers could not perform the task even though their grating detection threshold is low. Our cyclopean grating subtended 6x6 deg.

To investigate the conflict between our conclusion and those of Harris & Watamaniuk (1996), we repeated the exact conditions of the Harris & Watamaniuk experiment and obtained results similar to their results. Although we cannot rule out the possibility that their two observers were similar to the few we found who could not discriminate cyclopean speed, it seems more likely that the explanation lies in the very small size of their cyclopean grating (0.38deg x 3.06deg). It is known that cyclopean receptive fields are rather large, and it seems not unlikely that cyclopean bars only 0.38deg long would be an ineffective stimulus for the cyclopean mechanism, These findings were reported at ARVO[18] and published in *Vision Research.*[15]

2.4 Visual processing of the direction of motion in depth.

Relevance: As for Sections 2 above.

Long-Term Aims 1.1.1(a), 1.1.1(c), 1.1.2(a), 1.1.(c); Specific Aims 1.2.9(a)-(c).

Three papers and one book chapter have been published:

Portfors-Yeomans, C. V. & Regan, D. (1997). Discrimination of the direction and speed of a monocularly-visible target from binocular information alone. J. Exp. Psychol.: Hum. Percept & Perform. 23, 227-243. Portfors-Yeomans, C. V. & Regan, D. (1996). Cyclopean discrimination thresholds for the direction and speed of motion in depth. Vision Research. 36, 3625-3279. Portfors-Yeomans, C. V. & Regan, D. (1997). Just-noticeable difference in the speed of cyclopean

motion in depth and of cyclopean motion within a frontoparallel plane. Journal of Experimental Psychology: Human Perception & Performance. *23, 1074-1086. Regan, D., Gray, R., Portfors, C. V., Hamstra, S. J., Vincent, A., Hong, X. H., and Kohly, R. (1998). Catching, hitting, and collision avoidance. In L. Harris & M. Jenkin (Eds.),* Vision and Action. *New York: Cambridge University Press, 171-209.*

In Fig. 22(A) the left and right eyes (LE, RE) fixate a nonious line (N) that forms part of a reference plane. At time t = 0 a target (T) is located on a line that is normal to the frontal plane and passes through point C midway between the eyes. Target T is located at distance D from point C, and is some distance in front of a reference plane of stationary marks. Target T is moving at a constant speed V along a straight line (bold arrow). At time t = Δt, target T will have moved through an absolute distance $V\Delta t$. Consequently, the angle between the retinal images of the target and any given mark in the stationary reference plane will change by $(\Delta\phi)_L$ in the left eye and $(\Delta\phi)_R$ in the right eye. If we let $\Delta t \rightarrow 0$ we can write the associated instantaneous rates of change as $(d\phi/dt)_L$ and $(d\phi/dt)_R$.

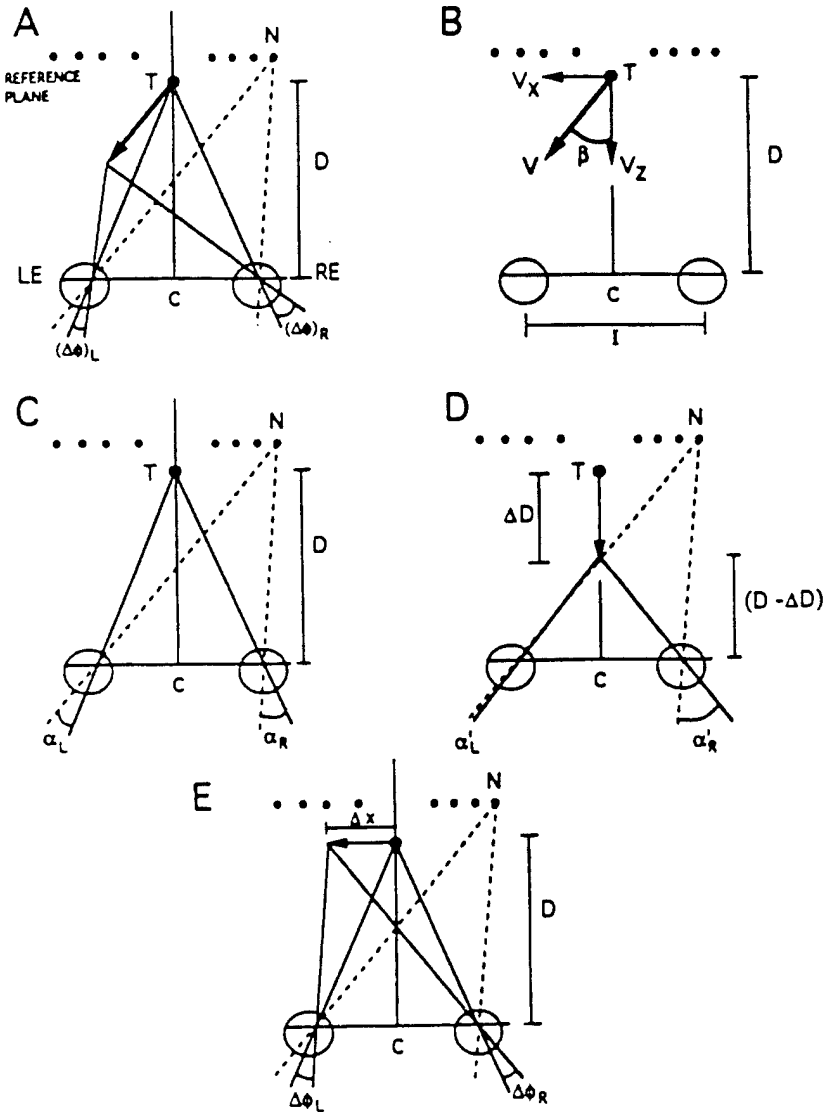

Figure 22. Geometry of motion in depth of a target (T) within a plane containing the left and right eyes. See text for details.

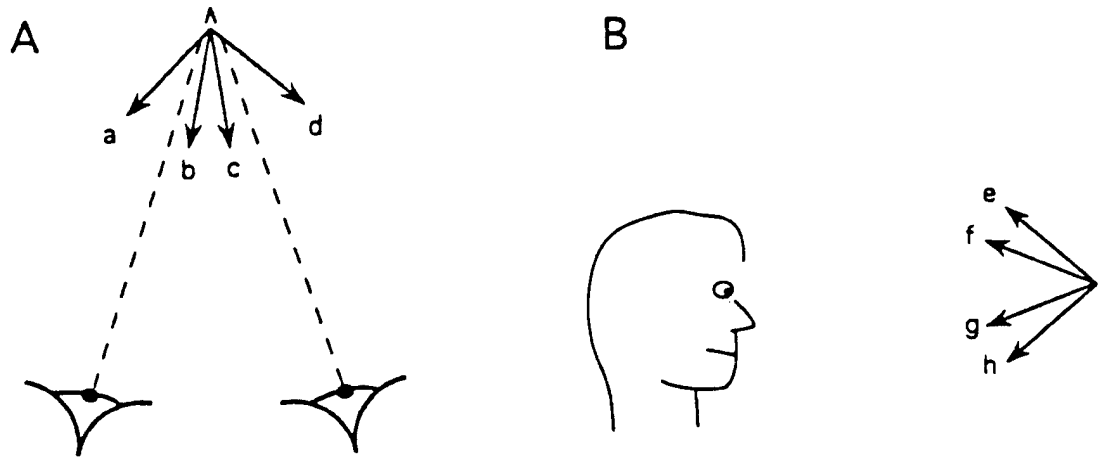

Figure 23. (A) Different directions of motion within a plane that contains the left and right eyes is normal to the frontal plane. For brevity, we will refer to this as motion within the horizontal meridian. (B) Different directions of motion within the vertical meridian.

Fig. 22(B) illustrates how the velocity (**V**) of target T can be resolved into the following two orthogonal components: a component of magnitude V_Z along direction TC (where $V_Z = V\sin\beta$), and a component of magnitude V_X parallel to the frontal plane (where $V_X = V\cos\beta$). It will be convenient to discuss these two components separately.

Fig. 22(C) illustrates that, at time t = 0, the disparity of target T relative to mark (N) in the reference plane is given by $\delta = \alpha_R - \alpha_L$. Fig . 22(D) illustrates that, at time $t = \Delta t$, the V_Z component of the target's motion has reduced the distance TC from D to (D-ΔD), and the instantaneous disparity of target T relative to mark N is now given by $\delta' = \alpha'_R - \alpha'_L$. The disparity displacement is $\Delta\delta$, where $\Delta\delta = (\delta' - \delta)$. (Note that this displacement is the same for any given

mark in the reference plane). If we let $\Delta t \rightarrow 0$ we can write the associated instantaneous rate of change of disparity as $d\delta/dt$.

Fig. 22(E) shows that at time $t = \Delta t$, the V_X component of the target's motion has translated the target through distance Δx. This will alter the angular distance between the left eye's retinal image of the target and the left eye's retinal image of mark N by an amount $\Delta\phi$. Approximately the same change will occur in the right eye's retinal image. If we let $\Delta t \rightarrow 0$ we can write the associated instantaneous rate of change as $(d\phi/dt)$.

For motion contained within a plane that contains the eyes and is normal to the frontal plane, the magnitudes of the ratio $(d\phi/dt)/(d\delta/dt)$ and the ratio $(d\phi/dt)_R/(d\phi/dt)_L$ both vary with the direction of motion in depth. For example, both ratios vary as direction is changed from *a* through *d* in Fig. 23(A). For convenience we will term this case "motion within the horizontal meridian" . The situation is different for motion confined to the vertical meridian in that the magnitude of $(d\phi/dt)/(d\delta/dt)$ varies as direction is changed from *e* through *h* in Fig. 23(B), but the ratio $(d\phi/dt)_R/(d\phi/dt)_L$ remains constant.

In particular, there are two binocular correlates of the direction of motion in depth for a straight-ahead monocularly-visible target whose motion is confined to the horizontal meridian [Fig. 23(A)]. First, the direction of an object's motion in depth [β in Fig. 23(B)] is given by,

$$\beta \approx \tan^{-1}\left\{ \frac{I\{[(d\phi/dt)_R/(d\phi/dt)_L]+1\}}{2D\{[(d\phi/dt)_R/(d\phi/dt)_L]-1\}} \right\} \text{----------} \quad (4)$$

(provided that D>>I), where $(d\phi/dt)_R$ and $(d\phi/dt)_L$ are, respectively, the translational angular velocities of the object's retinal images in the right and left eyes, D is the object's distance and I is the observer's interpupillary separation (Beverley & Regan, 1973, 1975; Regan, 1986, 1993). However, even for monocularly-visible targets the $(d\phi/dt)_R/(d\phi/dt)_L$ cue is available only for motion contained within the horizontal meridian. A second binocular correlate of β is given by equation (5):

$$\beta \approx \tan^{-1}\left[\frac{I(d\phi/dt)}{D(d\delta/dt)} \right] \text{----------} \quad (5)$$

(again provided that D>>I), where $(d\phi/dt)$ is the angular velocity of the binocularly-fused retinal image. (More exactly this is the angular velocity of the target's fused retinal image relative to the retinal image of some fixed reference mark. It is equal to $0.5[(d\phi/dt)_R + (d\phi/dt)_L]$, see Fig. 22A). The quantity $(d\delta/dt)$ is the target's rate of change of relative disparity (Regan, 1993). This correlate is available for motion within any meridian. It is the only correlate of the direction of motion in depth for cyclopean targets.

It has been pointed out that, for an approaching object whose instantaneous location is straight ahead, this representation of the direction of motion in depth directly indicates the point of arrival in the plane of the eyes

(in particular whether the object will hit the observer's head), and that this property is independent of the direction of gaze and the angle of convergence (Beverley & Regan, 1973). This property follows from the fact that I/D radians is the angle subtended by the distance between the eyes from the viewpoint of the approaching object. In many everyday situations, and certainly in terms of evolutionary pressures, this information is considerably more important to the observer than is the ability to estimate the value of β. [Turning back to our sporting context, equation (5) indicates where (in units of I) a catcher's hand should be placed to intercept a ball passing over, under, or to the side of the head]. If we express in these terms the directional thresholds for monocularly-visible targets reported by Beverley and Regan (1973) and Portfors-Yeomans and Regan (1996), discrimination threshold for the point of impact of an approaching object is lowest for impact midway between the eyes and has a value of approximately 0.2 cm in the plane of the face, i.e. approximately 0.03I assuming I = 6 cm. If, as seems to be the case (Portfors-Yeomans & Regan, 1996), visual processing of the terms in square brackets in equation (5) is independent of viewing distance, direction discrimination threshold expressed in terms of I will be independent of the approaching object's distance (providing that the speed of the approach is sufficiently high to raise $d\delta/dt$ well above threshold).

We previously reported that discrimination threshold for the direction of motion in depth for a monocularly-visible target moving in the horizontal meridian was 0.2 deg (Beverly & Regan, 1975). More recently we found that discrimination threshold was the same for motion within the vertical and

horizontal meridian (Portfors-Yeomans & Regan, 1997). Given that the ratio of the left and right eyes' retinal image speeds provides no cue to the direction of motion in depth for motion within the vertical meridian, thus finding is consistent with the idea that, for motion within both horizontal and vertical meridians, discrimination is based on the ratio $(d\phi/dt)/(d\delta/dt)$.

We addressed this question by measuring discrimination threshold for the direction of motion in depth for a cyclopean target (Portfors-Yeomans & Regan, 1996). Our rationale was that the ratio between a cyclopean target's retinal images provides no cue to the direction of motion in depth, because the target is not visible monocularly. The set of 64 stimulus comprised different combinations of the direction of motion in depth [i.e. $I(d\phi/dt)/D(d\delta/dt)$] and $d\delta/dt$, $d\phi/dt$ and $\Delta\delta$. Following each presentation, observers were instructed to signal (a) whether the direction of motion in depth was directed wider of the head than the mean direction of the stimulus set, and (b) whether the speed of motion in depth was faster than the mean of the stimulus set. Observers based their direction discriminations entirely on the task-relevant variable $I(d\phi/dt)/D(d\delta/dt)$, and ignored all task-irrelevant variables. They based their speed discriminations entirely on the task-relevant variable (i.e. speed), and ignored all task-irrelevant variables. Performance on both tasks was the same for motion within vertical and horizontal meridians. We repeated the experiment using a monocularly-visible target that was created by switching off all dots outside the cyclopean target. Thresholds were either the same or only slightly different for the cyclopean and monocularly-visible targets. We

concluded that discrimination of the direction of motion in depth is determined by a mechanism sensitive to the ratio $(d\phi/dt)/(d\delta/dt)$ for both cyclopean and monocularly-visible targets. We also concluded that a single speed-sensitive mechanism determines speed discrimination threshold for both cyclopean and monocularly-visible targets.

Discrimination threshold for the direction of motion in depth of a monocularly-visible target can be as low as 0.14 to 0.2 deg (Beverley & Regan, 1975; Portfors-Yeomans & Regan, 1997). To explain this remarkably acute performance, Beverley and Regan (1975) proposed that the human visual pathway contains neural mechanisms tuned to different directions of motion in depth, and that the relative activity of these mechanisms determines discrimination threshold. The obtained evidence for such mechanisms by exploiting the finding that inspecting a monocularly-visible target moving along a line inclined in depth elevates threshold for detecting motion in depth, but only for a limited range of test directions (Beverley & Regan, 1973). These experiments, however, were restricted to motion in depth within the horizontal meridian so that it was not clear whether the proposed mechanisms were selectively tuned to the ratio $(d\phi/dt)_R/ (d\phi/dt)_L$, to the ratio $(d\phi/dt)/(d\delta/dt)$, or to some combination of the two.

More recently we repeated and extended these experiments by using a cyclopean target, and using motion within both the vertical and horizontal meridian [Regan & Portfors, ARVO 1997, Ref. 7(a)3]. Fig. 24 (A) shows baseline (preadaptation) thresholds for detecting oscillations of a cyclopean target along

9 test directions of motion in depth within the horizontal meridian. Fig. 24(G) shows similar data for motion within the vertical meridian. Fig. 24(B) - (F) shows threshold elevations caused by adapting to motion along 9 test directions within the horizontal meridian (arrowed on abscissae). Fig. 24(H) - (L) show corresponding threshold elevations for motion within the vertical meridian.

The lines in Fig. 24(A) -(L) join the data points. The lines in Fig. 25(A) - (L) were derived theoretically from the sensitivity profiles shown in Fig. 26(A) & (B), using a simulation procedure described by Tyler, Barghout & Kontsevich (1996). Except for panels (F) & (L), the fits are tolerably close.

The profiles for the cyclopean mechanisms sensitive to motion within the horizontal meridian [Fig. 26(A)] are quite similar to the sensitivity profiles inferred by Beverley & Regan (1973) for mechanisms tuned to the direction of motion in depth within the horizontal meridian of a monocularly-visible target.

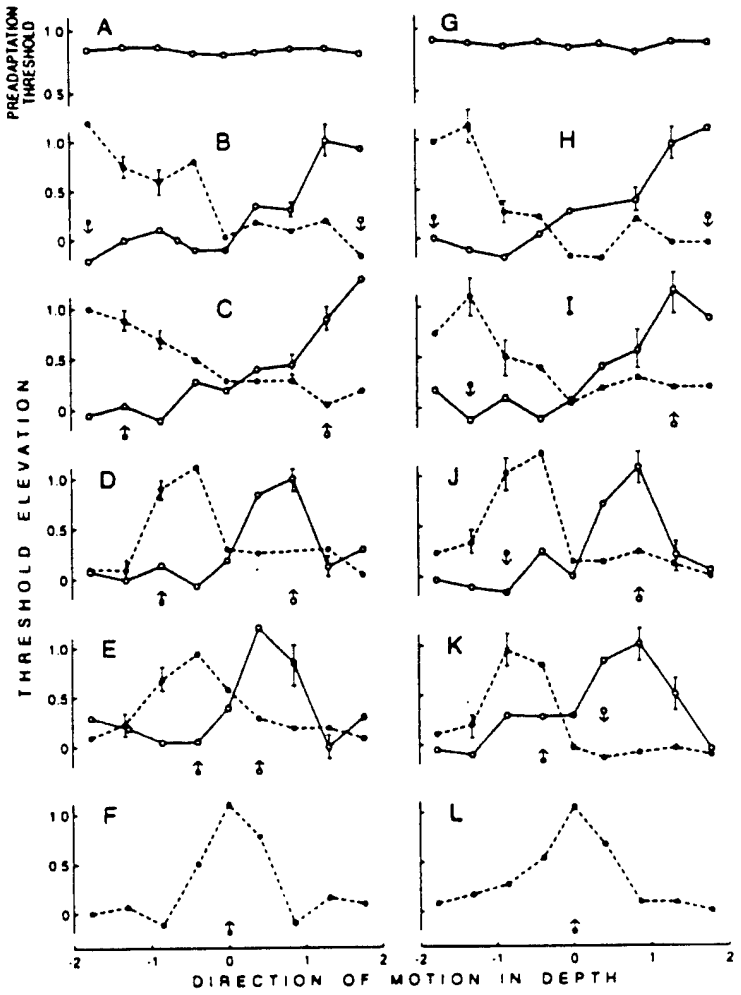

Figure 24. Preadaptation and postadaptation thresholds for detecting the motion in depth of a cyclopean target moving with a horizontal meridian (A - F) and within a vertical meridian (G - L). A, G: Normalized preadaptation thresholds (ordinate) plotted versus the ratio $(d\phi/dt)/(d\delta/dt)$. B - F, H- L: Data points plot threshold elevations caused by adapting to different directions of motion in depth (arrowed). Positive values of $(d\phi/dt)/(d\delta/dt)$ mean rightward in B - F and upward in H - L. Vertical bars indicate ± 1 standard errors. The lines join point to point and are intended to guide the eye.

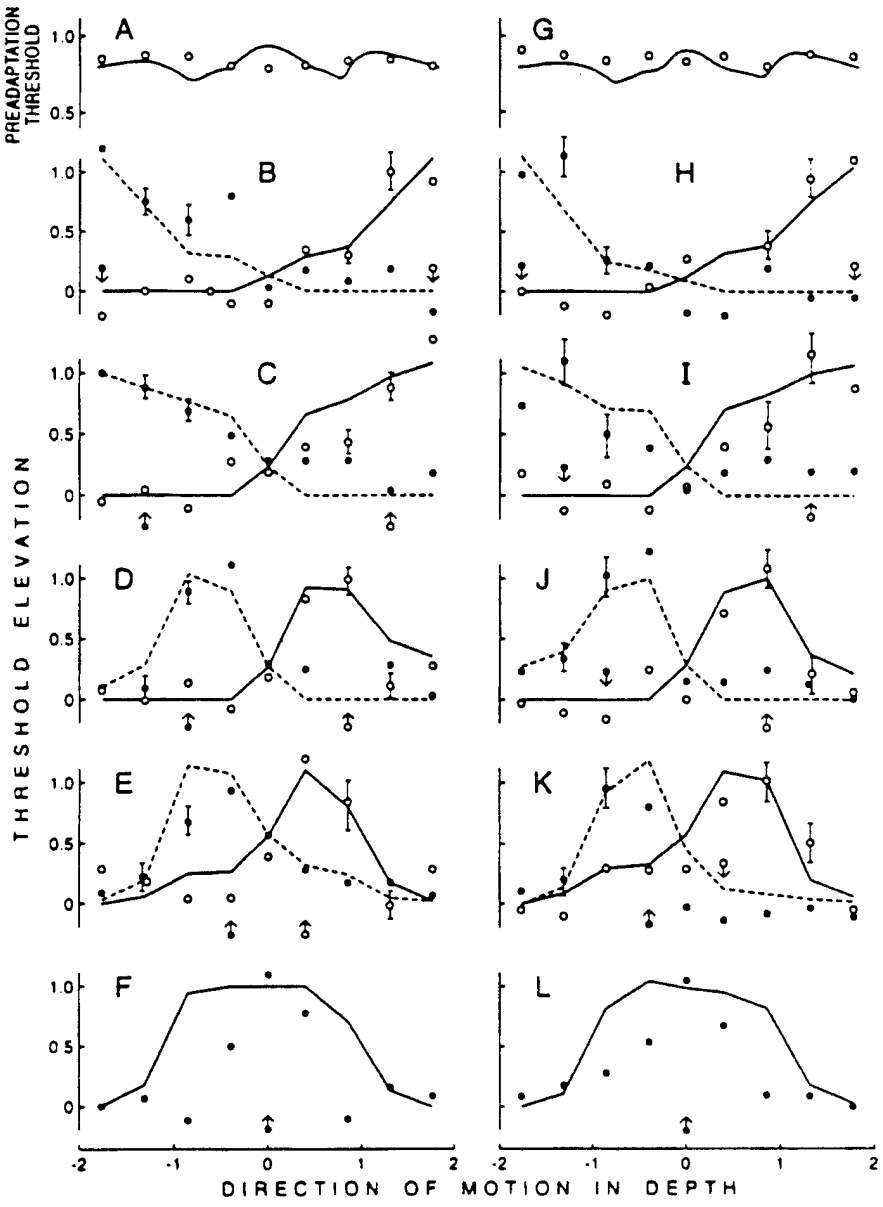

Figure 25. Same data as in Figure 20. The lines are theoretical prediction based on the profiles in Figure 26.

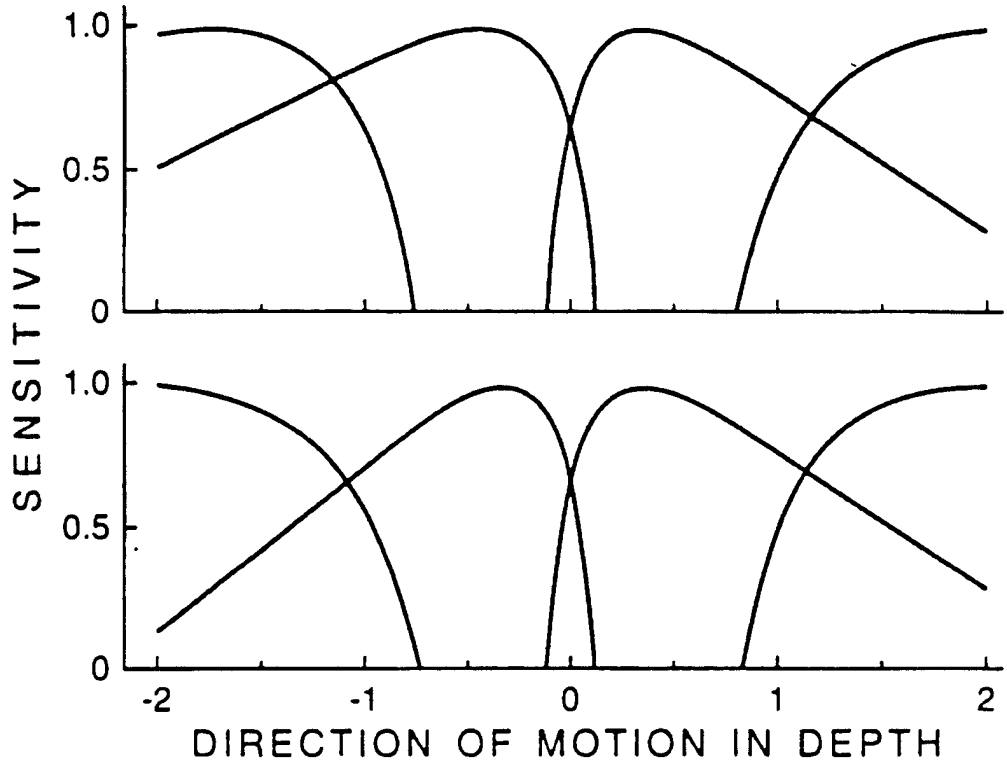

Figure 26. Plots of relative sensitivity (ordinate) versus direction for the proposed mechanisms that best predict the data shown in Figure 24 (A)–(L).

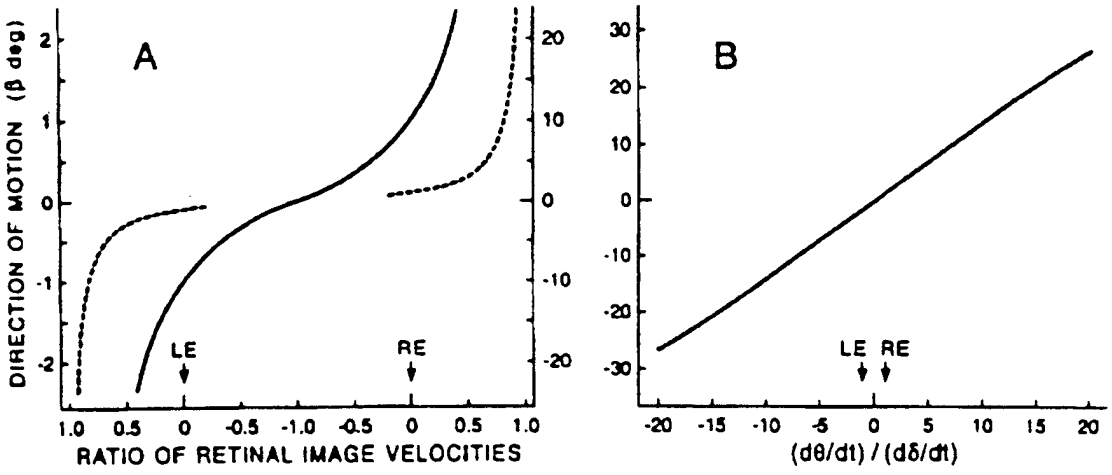

Figure 27. Direction of an object's motion in depth (ordinate) plotted versus the ratio between the velocities of the retinal images in right and left eyes (panel A), and (panel B) versus the ratio $(d\phi/dt)/(d\delta/dt)$. In panel A the left ordinate is for the continuous line and the right ordinate is for the broken line.

This finding supports our proposal that binocular information about the direction of motion in depth is processed by the same cyclopean mechanisms whether the target is monocularly -visible or cyclopean.

Calibration of cyclopean motion-in-depth mechanisms

Because the ratio $(d\phi/dt)/(d\delta/dt)$ indicates the direction of motion in depth for motion within any meridian, there is a clear advantage in encoding the direction of an object's motion in depth in terms of $(d\phi/dt)/(d\delta/dt)$ rather than in terms of the relative velocity of the object's left and right retinal images.

However, we are left to explain how the $(d\phi/dt)/(d\delta/dt)$ profiles align themselves to the particular directions of motion in depth that provide an optimal basis for judging whether an approaching object will pass to the left or right of the nose and whether it will hit or just miss the head (Beverley & Regan, 1975). For motion within the horizontal meridian, the magnitude of $(d\phi/dt)_R$ passes through zero as the direction of the approaching object's motion passes through the right eye, and the magnitude of $(d\phi/dt)_L$ passes through zero as the direction of the approaching object's motion passes through the left eye independently of the object's location, the direction of gaze and vergence angle. In contrast, the ratio $(d\phi/dt)/(d\delta/dt)$ offers no such convenient marker of trajectories that graze the right and left sides of the head (Fig. 27). Given that, during early visual development, our experience of moving objects is of

monocularly-visible objects, we propose that the conditions $(d\phi/dt)_R = 0$ and $(d\phi/dt)_L = 0$ are used to align the tuning of the horizontal-meridian $(d\phi/dt)/(d\delta/dt)$ mechanisms so that they prefer the appropriate directions of motion in depth, even though the mechanisms are cyclopean.

For motion within the vertical meridian we suggest that, in the absence of any other markers, the markers of absolute direction [$(d\phi/dt)_R = 0$ and $(d\phi/dt)_L = 0$] are used to align the meridian $(d\phi/dt)/(d\delta/dt)$ channels during early visual development.

Taken together, the channels for motion within the vertical and horizontal meridians are adequate to provide a basis for judging whether an approaching object will hit the observer's head, whatever the object's trajectory.

Binocular neurons tuned to the direction of motion in depth

Neurons that, in response to binocular stimulation, fire most strongly for a particular direction of motion in depth have been found in the visual cortex of cat (Cynader & Regan, 1978, 1982; Regan, Beverley & Cynader, 1979; Regan & Cynader, 1982; Spileers et al., 1990; Ohzawa, DeAngelis & Freeman, 1996) and monkey (Poggio & Talbot, 1981). For motion within the horizontal meridian, a candidate physiological basis has been found for each of the four pairs of mechanisms proposed by Beverley and Regan (1973). In particular, all of the following kinds of neural response preferences have been reported: an approaching target moving along a line directed wide of the left eye, directed between the left eye and the nose, directed between the nose and the right eye

and directed wide of the right eye; a receding target moving along one of the same four directions.

In the physiological reports just cited, the neural tuning was discussed in terms of the ratio $(d\phi/dt)_R$ / $(d\phi/dt)_L$ and the tuning curves were plotted in the polar coordinate system introduced by Cynader and Regan (1978). According to this coordinate system, the ratio between the left and right retinal image velocities is plotted as a linear function of azimuth, and radial distance is a function of neural response. In the light of the findings discussed in the present paper, we raise the possibility that, in all the papers just cited, both the discussion and the analysis of the physiological data was incomplete. For example, it can be inferred from Fig. 27 that neural tuning curves would look quite different when plotted as a function of $(d\phi/dt)$ /$(d\delta/dt)$ than when plotted in terms of the ratios between left and right retinal image velocities. As well, the mechanisms whose sensitivity profiles are depicted in figure 25(B) are tuned to the direction of motion in depth for motion within the vertical meridian. A hint that such neurons might exist was reported by Cynader and Regan (1978) who found that neurons that preferred oblique orientations were tuned to the direction of motion in depth within the vertical meridian. Perhaps this question might be resolved by investigating neural sensitivity to the direction of motion in depth using cyclopean targets rather than the monocularly-visible targets that have been used in all physiological studies to date.

2.4 Human brain electrophysiology

Long–Term Aim 1.1.4; Specific Aim 1.4.1. A paper was presented to ARVO in 1999 and a report is in preparation.

We optically superimposed two cyclopean gratings that were created within a pattern of dynamic random dots. For one grating (the reference grating) the bars exchanged positions in depth F_1 times per sec, while for the other grating (the variable grating) the bars exchanged positions in depth F_2 times per sec. We analyzed the electrical signals recorded from scalp electrodes by obtaining the power spectrum at a resolution of 0.004 Hz.

The rationale of this experiment is that any cross–modulation terms in the response (i.e. terms with frequencies $\{nF_1 \pm F_2\}$ Hz, where n and m are nonzero and integral, can only be generated by neurons that "see" both gratings. A cross–modulation term of frequency $(F_1 + F_2)$Hz was large when the variable and reference grating had the same orientation, and progressively fell to zero as the variable grating was rotated. Unlike the situation with luminance–defined gratings, cross–modulation terms were zero when the two gratings were orthogonal.

This is the first objective evidence for an orientation–tuned cyclopean neural mechanism in the human brain.

References to Accomplishments / New Findings

Adelson, E. H. & Bergen, J. R. (1985). Spatiotemporal energy models for the perception of motion. *Journal of the Optical Society of America*, 2, 284-299.

Bergen, J. R. & Adelson, E. (1988). Early vision and texture perception. *Nature (London)*, 333, 363-364.

Beverley, K. I., and Regan, D. (1973). Selective adaptation for stereoscopic depth perception. *Journal of Physiology*, 232, 40-41P.

Beverley, K. I., and Regan, D. (1975). The relation between discrimination and sensitivity in the perception of motion in depth. *Journal of Physiology*, 249, 387-398.

Beverley, K.I. & Regan, D. (1979a). Separable aftereffects of changing-size and motion-in-depth: different neural mechanisms? *Vision Research* 19, 727-32.

Beverley, K.I., & Regan, D. (1979b). Visual perception of changing-size: the effect of object size. *Vision Research, 19*, 1093-1104

Beverley, K.I. & Regan, D. (1980). Visual sensitivity to the shape and size of a moving object: implications for models of object perception. Perception 9,151-160.

Beverley, K.I., & Regan, D. (1983). Texture changes versus size changes as stimuli for motion in depth. *Vision Research, 23*, 1387-1400.

Blakemore, C. & Campbell, F. W. (1969). On the existence of neurons in the human visual system selectively sensitive to the orientation and size of retinal images. *Journal of Physiology*, 203, 237-260.

Bootsma, R. J., and van Wieringen, P. C. W. (1990). Timing an attacking forehand drive in table tennis. *Journal of Experimental Psychology: Human Perception and Performance*, 16, 21-29.

Campbell, F. W., Nachmias, J. & Jukes, J. (1970). Spatial-frequency discrimination in human vision. *Journal of the Optical Society of America*, 60, 555-559.

Cavallo, V., and Laurent, M. (1988). Visual information and skill level in time-to-collision estimation. *Perception*, 17, 623-632.

Collewijn, H. & Erkelens, C. J. (1990). Binocular eye movements and the perception of depth. In E. Kowler (Ed.) Eye Movements and their Role in Visual and Cognitive Processes (pp. 213-261). Amsterdam: Elsevier.

Cynader, M., and Regan, D. (1978). Neurons in cat prestriate cortex sensitive to the direction of motion in three-dimensional space. *J. Physiol.*, 274, 549-569.

Erkelens, C. J. & Collewijn, H. (1985a). Motion perception during dichoptic viewing of moving random-dot stereograms. *Vision Research*, 25, 583-588.

Erkelens, C. J. & Collewijn, H. (1985b). Eye movements and stereopsis during dichoptic viewing of moving random-dot stereograms. *Vision Research*, 25, 1689-1700.

Fiandt, K. von, & Gibson, J.J. (1959). The sensitivity of the eye to two kinds of continuous transformation of a shadow pattern. Journal of Experimental Psychology, 57, 344-347.

Fogel, I. & Sagi, D. (1989). Gabor filters as texture discriminators. *Biological Cybernetics*, 61, 103-113.

Gray, R. & Regan, D. (1998). Accuracy of estimating time to collision using binocular and monocular information. *Vision Research*, 38, 499-512.

Hong, X. H. & Regan D. (1989). Visual field defects for unidirectional and oscillatory motion in depth. *Vision Research*, 29, 809-819.

Hoyle, F. (1957). *The Black Cloud*. (pp. 26-27). London: Penguin books.

Heuer, H. (1993). Estimates of time to contact based on changing size and changing target vergence. *Perception*, 22, 549-563.

Johansson, G. (1964). Perception of motion and changing size. Scandinavian Journal of Psychology, 5, 181-208.

Klein, S. & Levi, D. M. (1985). Hyperacuity thresholds of 1 sec: theoretical interpretations and empirical validation. *Journal of the Optical Society of America*, A2, 1170-1190.

Landy, M. S. & Bergen, J. R. (1991). Texture segregation and orientation gradient. *Vision Research*, 31, 679-691.

Matin, L. (1972). Eye movements and perceived visual duration. In Jameson, D. & Hurvich, L.M. (Eds), *Visual psychophysics* (pp.331-380). New York: Springer.

Morgan, M. J. (1991). Hyperacuity. In Regan, D. (Ed.), *Spatial vision* (pp. 87-113). London: Macmillan and Baton Rouge: CRC Press.

Morgan, M. J. & Regan, D. (1987). Opponent model for line interval discrimination: interval and vernier performance compared. *Vision Research* , 27, 107-118.

Ohzawa, I., DeAngelis, G. C., and Freeman, R. D. (1996). Encoding of binocular disparity by simple cells in the cat's visual cortex. *J. Neurophysiol.*, 75, 1779-1805.

Poggio, G., and Talbot, W. H. (1981). Neural mechanisms of static and dynamic stereopsis in foveal striate cortex of rhesus monkeys. *J. Physiol.*, 315, 469-492.

Poincaré, H. (1913). The Value of Science. New York: Science Press.

Regan, D. (1982). Visual information channeling in normal and disordered vision. *Psychological Review, 89*, 407-444.

Regan, D. (1986). Binocular correlates of the direction of motion in depth. *Vision Research*, 33, 2359-2360.

Regan, D. (1995). Orientation discrimination for texture-defined form. *Perception*, 24, 1131-1138.

Regan, D., & Beverley, K.I. (1978a). Looming detectors in the human visual pathway. *Vision Research, 18*, 415-21.

Regan, D., & Beverly, K.J. (1978b). Illusory motion in depth: aftereffect of adaptation to changing size. *Vision Research, 18*, 209-212.

Regan, D., & Beverley, K.I. (1979a). Visually guided locomotion: psychophysical evidence for a neural mechanism sensitive to flow patterns. *Science, 205*, 311-313.

Regan, D., & Beverley, K.I. (1979b). Binocular and monocular stimuli for motion in depth: changing-disparity and changing-size feed the same motion-in-depth stage. *Vision Research, 19*, 1331-42.

Regan, D., & Beverley, K.I. (1980). Visual responses to changing size and to sideways motion for different directions of motion in depth: linearization of visual responses. *Journal of the Optical Society of America, 11*, 1289-96.

Regan, D., & Beverley, K.I. (1981). Motion sensitivity measured by a psychophysical linearizing technique. *Journal of the Optical Society of America, 71*, 958-65

Regan, D & Beverley, K.I. (1983). Spatial frequency discrimination and detection: comparison of post-adaptation thresholds. *Journal of the Optical Society of America, 73*,1684-1690.

Regan, D., and Cynader, M. (1982). Neurons in cat visual cortex tuned to the direction of motion in depth: effect of stimulus speed. *Investigative Ophthalmology and Visual Science*, 22, 535-550.

Regan, D. & Hong, X. H. (1996). Two-dimensional aspect ratio discrimination and one-dimensional width and height discriminations for shape defined by orientation texture. *Biological Cybernetics*, 72, 389-396.

Regan, D., & Vincent A. (1995). Visual processing of looming and time to contact throughout the visual field. *Vision Research, 35*, 1845-1857.

Regan, D., Beverley, K. I., and Cynader, M. (1979). The visual perception of motion in depth. *Scientific American*, 241, 136-151.

Regan, D., Erkelens, C. J. & Collewijn, H. (1986). Necessary conditions for the perception of motion in depth. *Investigative Ophthalmology Visual Science*, 27, 584-597,

Regan, D., Hajdur, L. V. & Hong, X. H. (1996). Two-dimensional aspect ratio discrimination and one-dimensional width and height discriminations for shape defined by orientation texture. *Vision Research, 36*, 3695-3702.

Regan, D., Kaufman, L. & Lincoln, J. (1986). Motion in depth and visual acceleration. In K.R. Boff, L. Kaufman and J.P. Thomas (Eds.) *Handbook of Perception and Human Performance*, Wiley: New York, p.19-1 to 19-46.

Regan, D., Erkelens, C.J. & Collewijn, H. (1986). Necessary conditions for the perception of motion in depth. *Invest Ophthalmol* Vis Sci 27, 584-97.

Rivest, J. & Cavanagh, P. (1996). Localizing contours defined by more than one attribute. *Vision Research*, 36, 53-66.

Rubenstein, B. S. & Sagi, D. (1990). Spatial variability as a limiting factor in texture-discrimination tasks: implications for performance asymmetries. *Journal of the Optical Society of America A*, 7, 1632-1643.

Schiff, W., & Detwiler, M. L. (1979). Information judged in impending collision. *Perception, 8*, 647-658.

Spileers, W., Orban, G. A., Gulyas, B., and Maes, H. 1990. Selectivity of cat area 18 neurons for direction and speed in depth. *J. Neurophysiol*, 63, 936-954.

Sutter, A, Beck, J. & Graham, N. (1989). Contrast and spatial variables in texture segregation: testing a simple spatial-frequency channels model. *Perception & Psychophysics*, 46, 312-332.

Tresilian, J. R. (1995). Perceptual and cognitive processes in time-to-contact estimation: analysis of prediction-motion and relative judgement tasks. *Perception & Psychophysics*, 57, 231-245.

Tyler, C. W. (1975). Characteristics of stereomovement suppression. *Perception & Psychophysics*, 17, 225-230.

Tyler, C. w. (1991). Cyclopean vision. In D. Regan (Ed.), *Binocular vision*, (pp. 38-74). London: Macmillan and Baton Rouge: CRC Press.

Vincent, A. & Regan, D. (1997). Judging the time to collision with a simulated textured object: effect of mismatching rates of expansion of size and of texture elements. *Perception and Psychophysics* 59, 32-36.

Watt, R. J. & Morgan, M. J. (1984). Spatial filters and the localization of luminance changes in human vision. *Vision Research*, 24, 1387-1397.

Westheimer, G. (1979). The spatial sense of the eye. *Investigative Ophthalmology and Visual Science*, 23, 1465-1477.

Westheimer, G. (1981). Visual Hyperacuity In Progress in Sensory Physiology vol. 1 pp.1-30. New York: Springer Verlag.

Westheimer, G. & McKee, S. P. (1977). Spatial configurations for visual hyperacuity. *Vision Research*, 17, 941-947.

Wheatstone, C. (1852). Contribution to the physiology of vision. II. Philosophical Transactions of the Royal Society (London), 142, 1-18.

Wilson, H. R. (1985). Discrimination of contour curvature: data and theory. *Journal of the Optical Society of America, A, 2,* 1191-1199.

Wilson, H. R. (1986). Responses of spatial mechanisms can explain hyperacuity. *Vision Research*, 26, 453-469.

Wilson, H. R. (1991). Psychophysical models of spatial vision and hyperacuity. In D. Regan (Ed.), *Spatial Vision* (pp. 64-86). London: Macmillan.

Wilson, H. R. & Regan, D. (1984). Spatial frequency adaptation and grating discrimination predictions of a line-element model. *Journal of the Optical Society of America*, A1, 1091-1096.

3. PROFESSIONAL PERSONNEL SUPPORTED BY OR ASSOCIATED WITH THE RESEARCH EFFORT

Dr. D. Regan Ph. D., D. Sc. (Physics).

Dr. X. H. Hong Ph. D. (Engineering).

Dr. M. P. Regan Ph. D. (Mathematics).

Mr. R. Gray M. A. (Psychology). Awarded Ph.D. Sept. 1998. Now at Nissan Basic Research, Boston (A lab supervised by Faculty at MIT and Harvard).

Ms. R. Kohly M.A (Psychology). Awarded M.A. Sept. 1998. Ph.D. (Biology) student.

Ms. C. V. Portfors (Biology). Awarded Ph.D. Sept. 1997).

Ms. L. Kwan B. A. (Psychology). Research Assistant.

4. PUBLICATIONS.

4.1 Papers in peer-reviewed journals

(1) Gray, R. & Regan, D. (1997). Vernier step acuity and bisection acuity for texture-defined form. *Vision Research*, 37, 1713-1723.

(2) Gray, R. & Regan, D. (1997). Spatial frequency discrimination and detection characteristics for gratings defined by orientation texture. *Vision Research, 38, 2601-2617.*

(3) Gray, R. & Regan, D. (1997). Estimating time to collision using binocular retinal image information alone, monocular retinal image information alone and a combination of the two. *Vision Research*, 38, 499-512.

(4) Vincent, A. & Regan, D. (1997). Judging the time to collision with a simulated textured object: effect of mismatching rates of expansion of size and of texture elements. *Perception and Psychophysics* 59, 32-36.

(5) Portfors-Yeomans, C. V. & Regan, D. (1997). Discrimination of the direction and speed of a monocularly-visible target from binocular information alone. *J. Exp. Psychol.: Hum. Percept & Perform.* 23, 227-243.

(6) Portfors-Yeomans, C. V. & Regan, D. (1997). Cyclopean discrimination thresholds for the direction and speed of motion in depth. *Vision Research.* 36, 3625-3279.

(7) Portfors-Yeomans, C. V. & Regan, D. (1997). Just-noticeable difference in the speed of cyclopean motion in depth and of cyclopean motion within a frontoparallel plane. *J. Exp. Psychol.: Hum. Percept & Perform.* 23, 1074-1086.

(8) Regan, D (1997). Visual factors in catching and hitting. *J Sports Sciences,* 15, 533-558.

(9) Giaschi, D., Lang, A. & Regan, D. (1997). Reversible Dissociation of sensitivity to dynamic stimuli in Parkinson's disease: Is magnocellular function essential to reading motion-defined letters. *Vision Research* 37, 3531-3534.

(10) Giaschi, D. & Regan, D. (1997). The development of motion-defined figure-ground segregation in preschool and older children using a letter-identification task. *Optometry & Vision Science,* 74, 761-767.

(11) Voisin, A., Elliott, D. B. & Regan, D. (1997). Babe Ruth: With vision like that, how could he play baseball? *Optom. & Vis Sci,* 74, 144-46.

(12) Kwan, L. & Regan, D. (1998). Orientation - tuned spatial filters for texture - defined form. *Vision Research* , 38, 3849-3855.

(13) Gray, R. & Regan, D. (1999). Adapting to expansion increases perceived time to collision. *Vision Research,* 39, 3602-3607.

(14) Gray, R. & Regan, D. (1999). Motion in depth: adequate and inadequate simulation. *Perception and Psychophysics,* 61, 236-245.

(15) Kohly, R. & Regan, D. (1999). Evidence for a mechanism sensitive to the speed of cyclopean form. *Vision Research,* 39, 1011-1024.

(16) Gray, R. & Regan, D. (1999). Estimating time to collision with a rotating nonspherical object. *Vision Research,* in press.

4.2 Book Chapters

(17) Regan, D. (1997). Perceptual motor skills and human motion analysis. In Handbook Of Human Factors And Ergonomics, G. Salvendy (Ed.) New York: Wiley. 174-218.

(18) Regan, D., Gray, R., Portfors, C. V., Hamstra, S. J., Vincent, A., Hong, X. H., and Kohly, R. (1998). Catching, hitting, and collision avoidance. In L. Harris & M. Jenkin (Eds.), Vision and Action. New York: Cambridge University Press, pp. 171-209.

4.3 Single-author book

Regan, D. (2000). Human Perception of Objects: early visual processing of spatial form defined by luminance, color, texture, motion and binocular disparity. Sunderland, MA: Sinauer, in press.

5. INTERACTIONS / TRANSITIONS

5 (a) Presentation at meetings, seminars etc.

(1) Gray, R. & Regan, D. (1997). Vernier step acuity and bisection acuity for texture-defined form. Investigative Ophthalmology & Visual Science, 38.4,(1997), S635. Presented at ARVO.

(2) Kohly, R.P., Hajdur, L.V., & Regan, D. (1997). There is a cyclopean speed-sensitive mechanism. Investigative Ophthalmology & Visual Science 38.4 (1997), S906. Presented at ARVO.

(3) Regan, D., Portfors, C.V. & Hong, X.H. (1997). Cyclopean mechanisms for the direction of motion in depth. Investigative Ophthalmology & Visual Science 38.4 (1997), S1168. Presented at ARVO.

(4) Regan, D. (1997). Hitting, catching, and collision avoidance. Presented to International Meeting on "Vision and Action", York University, June 1997.

(5) Kohly, R.P. & Regan, D.:

The Association for Research in Vision and Ophthalmology, Annual Meeting, Fort Lauderdale, FL, May 12, 1998.

- *Independent Encoding of Speed and Displacement for a Moving Cyclopean Grating,*

(6) Regan, D. & Kwan, L.:

The Association for Research in Vision and Ophthalmology, Annual Meeting, Fort Lauderdale, FL, May 13, 1998.

- *Orientation–Tuned Spatial Mechanisms for Texture–Defined Form.*

(7) Gray, R, & Regan, D.:

The Association for Research in Vision and Ophthalmology, Annual Meeting, Fort Lauderdale, FL, May 14, 1999.

- *The Relevance of Heading and Motion–in–depth Data Collected with Constant–Sized Dot Displays.*

(8) Kohly, R. & Regan, D:

The Association for Research in Vision and Ophthalmology, Annual Meeting, Fort Lauderdale, FL, May 9, 1999.

- *Coincidence Detectors with outputs labeled with orientation difference and mean orientation.*

(9) Regan, M.P., Hong, X.H., & Regan, D.:

The Association for Research in Vision and Ophthalmology, Annual Meeting, Fort Lauderdale, FL, May 11, 1999.

- *Orientation tuning of cyclopean mechanism in human measured objectively by exploiting nonlinearity.*

(10) Steeves, J., Gray, R., Regan, D., & Steinbach, M.J.:

The Association for Research in Vision and Ophthalmology, Annual Meeting, Fort Lauderdale, FL, May 13, 1999.

- *Accuracy of estimating time to collision using only monocular information in unilaterally enucleated observers and monocularly viewing normal controls.*

(11) Gray, R., & Regan, D.:

The Association for Research in Vision and Ophthalmology, Annual Meeting, Fort Lauderdale, FL, May 13, 1999.

- *Estimating time to collision with a rotating nonspherical object.*

5(b) Consultative and advisory functions.

5(b)1 Consultation and advice on the design and the use for training of compact flight simulators and on the design of experiments to investigate possible limitations in collaboration with Dr. Byron Pierce and Dr. George Geri, Armstrong Lab., U.S.A.F. The background is that simulators have been developed in which left and right eyes view binocularly a display that is only 1 - 2 m away and is not collimated. The display is not stereoscopic. At this close viewing distance in everyday life, binocular cues to time to collision and directions of motion in depth are available and, as we have shown in Refs. 3,5

&6, are used. The possibility arises that the high ocular convergence angle may cause the brain to "expect" binocular information, and its absence might cause errors of judgement.

5(b)2 Collaborative research on collision avoidance and on the terrain texturing requirements for nap-of-the-Earth (NOE) flight in helicopters using the Simulator Training Research Advanced Tested for Aviation (STRATA) at the Army Research Institute (ARI) at Fort Rucker, Alabama. Collaboration is with Dr. C. Gainer, Chief, Aviation Research and Development Activity, U. S. Army Research Institute, Fort Rucker. Data collection is organized by Dr. R. Kruk of CAE who installed the Fort Rucker stereo simulator. Dr. Kruk's travel and living expenses for his visits to Fort Rucker are paid entirely by CAE. Subjects on the simulator studies, apart from Dr. Kruk, are pilot instructors from Fort Rucker who volunteer their time gratis

5(b)3 Editorial Board: *Spatial Vision*

Editorial Board: *Ophthalmic and Physiological Optics*

Editorial Board: *Vision Research.*

5(b)4 Grant Reviewer: National Eye Institute (USA), Wellcome Trust (UK), Medical Research Council (UK).

5(b)5 Journal Reviewer: Vision Research, Nature, Percept. & Psychophysics, Human Factors, J. Sports Science, JOSA, Quarterly J. Exp. Psychol.

5(c) Transitions

See 7(b)1 above.

6. PATENTS

None.

7. HONORS / AWARDS

7.1 Awards during the grant period.

In June 1999 the P.I. was elected as a Foreign Member of the Netherlands Royal Academy of Science. In December 1998 the P.I. was elected to the Spinoza Chair for 1999 by the medical faculty of the University of Amsterdam, and gave the 5 Spinoza lectures in October 1999.

In May 1997, the P. I. was awarded the Sir John William Dawson medal, the highest honour of the Royal Society of Canada. This medal is awarded for "important and sustained contributions by on individual in at least two different domains." The citation listed contributions in Human Biology, Psychology, Medicine and Public Safety.

In 1998 the P.I. was elected a Fellow of the Canadian Psychological Association.

7.2 Lifetime achievement honours prior to grant period.

Charles F. Prentice Medal, American Academy of Optometry, 1990

Fellow of the Royal Society of Canada, 1989

D.Sc. (London University, 1974)

Distinguished Research Professor, York University, 1991

I.W. Killam Fellow, 1991

I.W. Killam Research Professor, 1978

Medical Research Council of Canada Lecture, 1990

Max Forman Prize for Medical Research

Fellow of the Optical Society of America

Fellow of the American Academy of Optometry

Listed in "Who's Who in America" ,"Canadian Who's Who" ,"American Men & Women of Science, "International Who's Who in Medicine", "Who's Who in Engineering", "Dictionary of International Biography"